NREL/TP-451-5756 • UC Category: 271 • DE93018214

Stable, High-Efficiency Amorphous-Silicon Solar Cells with Low Hydrogen Content

Final Subcontract Report
1 March 1991 – 31 March 1993

S. S. Hegedus, J. E. Phillips
Institute of Energy Conversion
University of Delaware
Newark, Delaware

NREL technical monitor: B. von Roedern

National Renewable Energy Laboratory
1617 Cole Boulevard
Golden, Colorado 80401-3393
Operated by Midwest Research Institute
for the U.S. Department of Energy
under Contract No. DE-AC02-83CH10093

Prepared under Subcontract No. XG-1-10063-4

August 1993

NOTICE

Printed in the United States of America
Available from:
National Technical Information Service
U.S. Department of Commerce
5285 Port Royal Road
Springfield, VA 22161

Price: Microfiche A01
Printed Copy A04

Codes are used for pricing all publications. The code is determined by the number of pages in the publication. Information pertaining to the pricing codes can be found in the current issue of the following publications which are generally available in most libraries: *Energy Research Abstracts (ERA)*; *Government Reports Announcements and Index (GRA and I)*; *Scientific and Technical Abstract Reports (STAR)*; and publication NTIS-PR-360 available from NTIS at the above address.

Printed on recycled paper

PREFACE

This report describes a 21 month project directed towards the demonstration of amorphous silicon solar cells with high stabilized conversion efficiency. The objective of this work was to develop a research program spanning material issues (more stable amorphous silicon and better amorphous silicon-germanium alloys) and device issues (more stable amorphous silicon based solar cells) towards the goal of high stabilized solar cell efficiency. To maintain consistency with the original statement of work, this report is grouped according to material. IEC has produced and analyzed the stability of amorphous silicon films and solar cells with reduced hydrogen content (2-6%). A thermodynamic model of defect formation was developed which describes the high temperature degraded state of a solar cell. Measurements of amorphous silicon and silicon-germanium films in collaboration with Pennsylvania State University and University of Oregon, have yielded conflicting results regarding the increase in Urbach energy and deep defect density with Ge alloying and the increase in defects with light exposure. Analysis of bifacial current voltage and quantum efficiency results for a-SiGe p-i-n devices having transparent front and back contacts has provided information about the influence of alloying and bandgap grading on hole and electron collection. Stability of graded and ungraded a-SiGe solar cells was also studied using bifacial devices to learn about the relative degradation of hole and electron collection.

SUMMARY

A. Objectives

The overall objective of the research described in this report was to develop amorphous silicon solar cells with high stabilized efficiencies. To achieve this goal, our intermediate objective was to resolve several key material and device issues. These key issues are: 1. whether a reduction in hydrogen content in amorphous silicon intrinsic layers can lead to higher stabilized solar cell efficiencies; 2. how the performance of solar cells made with narrow band gap a-SiGe:H can be enhanced; 3. how the particular materials and device parameters determine stabilized performance of a-Si:H solar cells; and 4. how particular materials and device parameters influence performance of a-SiGe:H based solar cells.

B. Principal Results and Conclusions

Amorphous silicon films were deposited by photo-CVD and plasma-CVD under conditions intended to reduce the hydrogen content to determine whether low hydrogen materials offered improved stability. The deposition of low hydrogen materials proved to be difficult. Low hydrogen films deposited by photo-CVD tended to flake or peel. The stability of samples that did not flake was measured by the change in Q.E. at 450 nm of Schottky solar cells or by photoconductivity. We found that stability was unrelated to hydrogen content in the range of 2-6%. However, stability of these low hydrogen films was better than standard a-Si films having >10% hydrogen.

A multichamber glow discharge reactor has become fully operational. Films were deposited as a function of hydrogen dilution and substrate temperature to obtain low hydrogen content (C_H=2-4%). We expect to use the glow discharge reactor for the fabrication of multi-junction solar cells. No difference in stability between photo-CVD or glow discharge was observed for films with 2-6% hydrogen.

In collaboration with the University of Neuchatel, the effects of high intensity rapid degradation was studied using devices from IEC and Neuchatel. The FF after rapid high intensity degradation was found to rapidly self anneal in the dark at room temperature, unlike the FF of devices exposed to one sun illumination for long intervals.

The self annealing of rapidly produced defects supports the thermodynamic equilibrium description of the Staebler-Wronski effect developed during this research. Perhaps the most important prediction of this description is that the dangling bond concentrations will stabilize at a level determined by the

temperature and illumination level. The thermodynamic description predicts that at low illumination levels the stabilized defect concentrations will be far less than the number of weak bonds, in contrast to a number of other popular defect models which predict that defects will form until all weak bonds are consumed.

To identify the means to improve amorphous silicon-germanium solar cells we first sought to better understand the range of material parameters of amorphous silicon-germanium films. Collaborations with the University of Oregon, Penn State University and the University of Rochester examined the alloy materials prepared by photo-CVD. Results from transient and steady state charge-release spectroscopy at University of Oregon suggest that the midgap defect density in our 1.4 eV a-SiGe films (Ge~45%) is about 5 times greater than in a-Si and increases by another factor of 3 with 200 hours light soaking, and the Urbach energy is 52 meV. Results from sub bandgap photoconductivity spectroscopy at Penn State suggests the midgap density is 10-30 times higher in our 1.4 eV a-SiGe films than in a-Si but has negligible increase with 100 hour light soaking, and the Urbach energy is 59 meV. These significant differences regarding stability could be due to unintentional differences in film quality or sensitivity of different measurements to different types of defects. This conflicting set of results indicates the difficulty of focussing on film-based measurements and the potential uncertainty of applying film-based results to interpreting device results.

A front loaded amorphous silicon germanium solar cell with an efficiency of 6% was made having 500Å of 1.3 eV a-SiGe and 500Å of a-Si.

We have studied simplified diagnostic p-i-n devices consisting of front loaded a-SiGe/a-Si or ungraded a-SiGe i-layers which have transparent front and back contacts for bifacial photocurrent measurements. This allows probing electron (hole) limited collection using strongly absorbed blue light through the p(n) layer. Both FF and QE(V) data indicate that the primary effect of grading the i-layer in the front loaded device is to improve hole collection rather than electron collection. However, electron collection degrades more than hole collection with extended light soaking (200 hours). **We conclude that device results do not agree with photoconductivity stability studies on a-SiGe films.** Stability studies of films show the electron $\mu\tau$ is unaffected by light soaking while device results suggest that electron collection degrades significantly.

The current voltage behavior of amorphous silicon and silicon germanium solar cells was analyzed to extract the lumped equivalent circuit parameters needed to represent the devices in a multi-junction configuration. The purpose of modeling was to

simplify and guide the design of multi-junction solar cells. Only fixed series resistance and shunt conductance terms were needed to represent the current voltage characteristics for this purpose. Analysis of both individual single junction cells and dual bandgap multijunction devices from Solarex indicates the component cells in the multijunction device have better performance than the individual single junctions, and there are no complications due to the np recombination junction.

An accidental release of hydrogen directly from a pressurized cylinder to the photo-CVD vacuum pump system resulted in an explosion on September 1, 1992. There were no injuries and damage was minimal. Both a-Si deposition reactors were shut down for the last four months of this contract. The cause was investigated by an outside team. Extensive improvements to the a-Si system and to the facility were recommended and implemented. A complete discussion is contained in Section 4. Without the capability to deposit special samples, a considerable number of research issues which were under study remained unresolved at the end of the contract.

LIST OF CONTRIBUTORS

TW Fraser Russell	Chemical Reaction Engineering Analysis of Photo-CVD
Wayne Buchanan	Photo-CVD Reactor Design, Material Preparation, Device Fabrication
Sarah Buchanan	Device Measurements
Ronald Dozier	Instrumentation and Measurements
Alissa Eggert	Depositions
Doug Darrell	Instrumentation
Diego Fischer	Device and Materials Analysis
Charles Fortmann	Material Deposition and Analysis
Richard Zielinski	Reactor Analysis and Depositions

TABLE OF CONTENTS

LIST OF FIGURES

LIST OF TABLES

SECTION 1.0

INTRODUCTION

Theoretical studies of multi-junction a-Si:H solar cells project efficiencies greater than 20%. Multi-junction solar cells offer the greatest potential for increased solar cell performance with acceptable long term stability. However, a number of problems will need to be remedied before the multijunction solar cell can achieve its full potential. The research presented here is directed towards the identification and rectification of these problems. First, this project seeks to determine why current material and device designs limit stabilized efficiencies to less than 10%. Secondly, we will use the understanding of existing materials to improve the stabilized efficiency of the amorphous silicon solar cells. Finally, we seek methods of depositing improved materials resulting in improved solar cell performance.

For example, multijunction solar cell stability is apparently controlled by the stability of the middle solar cell which, with present technology, must be made relatively thick to absorb a sufficient quantity of the solar spectrum. It has been reported by a number of groups that the stability of amorphous silicon solar cells decreases with increasing i-layer thickness. Therefore a portion of our research was directed towards finding ways to prepare more stable amorphous silicon solar cells which have relatively thick i-layers.

Problems with the red absorbing solar cell (the bottom cell of a triple stack) have also been identified. The need to efficiently convert the near infrared portion of the solar spectrum requires low band gap alloy, typically a-SiGe. Researchers have been able to improve the moderately low band gap (1.4-1.5 eV) a-SiGe alloy solar cells but the performance is still below expectation. These low gap solar cells limit the initial performance of the multijunction solar cell. The alloy solar cell could also become the limiting factor to stabilized efficiency of multijunction solar cells once more stable middle cells are incorporated.

This report covers years one and two of what was originally a three year program whose goal was the development of amorphous silicon based solar cells with a stabilized efficiency greater than 12%. The research program described here was largely, but not entirely, adopted in creating the new contract goals of the Institute of Energy Conversion, University Center of Excellence for Photovoltaic Research and Education. To establish a basis on which to achieve the goal of 12% stabilized efficiency, it was necessary to identify the best materials and single junction solar cell structures. In the future phases of this effort, these would become component cells of multi-junction solar cells.

During this segment of research our efforts were also directed towards identifying and characterizing state-of-the-art a-SiGe:H materials. These efforts sought to obtain a consistent set of material parameters from the characterization, analysis and measurement of films and devices. Due to the widespread disagreement between reported values for such basic quantities as the density of dangling bonds in a-SiGe:H, it is not possible to assume that reported values are applicable to our materials. It is also unclear whether defects or transport properties detected by a given measurement actually affects solar cell performance. We sought to establish a data base of materials characteristics with our own measurements and with measurements made in collaboration with other laboratories.

The present objectives are to develop the most stable materials, understand the underlying nature of the Staebler-Wronski effect in a-Si:H, and also to understand the transport phenomena in the Si-Ge alloy system in order to provide the later phases of this project with the materials and design parameters necessary to develop solar cells with greater stabilized efficiency. It is an integral part of our research program's objectives to examine low hydrogen materials. It is reported that high hydrogen materials are less stable than standard materials. The examination of low hydrogen materials also supports our other objectives. These materials offer three possibilities to enhance the performance and stability of multijunction amorphous silicon based solar cells. First, low hydrogen materials may be more stable than standard amorphous materials. Secondly, we know that hydrogen content and bonding configuration affect the band gap of amorphous materials. Band gap differences can be exploited by multijunction solar cell design to increase the performance. For example, a smaller band gap permits the use of a thinner i-layer in the middle solar cell of a triple stack device, thus enhancing its stability. Finally, we know that reduced hydrogen content in the silicon-germanium alloys improves the electronic transport.

Our long range goals require that two levels of computer modeling be developed in parallel with the materials effort. One level of modeling relates material parameters to single junction solar cell performance. The other level relates single junction solar cell parameters to multi-junction solar cell performance using the SPICE circuit analysis program. To assist in the modeling of stabilized device efficiency, we began by modeling the high temperature steady-state Staebler-Wronski effect. A new model based on classical thermodynamics was developed in collaboration with groups at Penn State, University of Oregon, and NREL. Relative material stability is predicted from extrapolation of the high temperature steady state to normal solar cell operating conditions.

A key feature of our research at IEC is the use of solar cells as diagnostic devices to learn about the materials. Previously, we

have reported results of using p-i-n solar cells to characterize midgap defect densities by capacitance, Urbach energies and light induced defects by sub-bandgap primary photocurrents, and light induced defects by short wavelength quantum efficiency. During this contract, we used p-i-n devices having transparent front and back contacts to make bifacial current voltage and spectral response measurements. The influence of alloying with Ge, graded i-layer composition, and light soaking on electron and hole transport in a-SiGe devices was studied with bifacial measurements.

SECTION 2.0

TASK 1 - STABILIZED a-Si:H MATERIALS AND DEVICES

2.1 INTRODUCTION TO LOW HYDROGEN MATERIALS

Our approach to improved stability during this contract was to investigate films and devices with reduced hydrogen content. Materials deposited by both our photo-CVD and plasma-CVD systems were studied. We have previously shown that our standard photo-CVD device i-layer, deposited at 205°C from SiH_4 and He at 5 Torr, has about 7% hydrogen content (1,2) and that it is more stable than photo-CVD films and devices having 11% hydrogen. Typical device quality plasma-CVD films have 10-15% hydrogen, so our standard photo-CVD i-layer is already lower in hydrogen and more stable than the industry standard.

During this contract we sought deposition conditions leading to a-Si material with 2-6% hydrogen. Hydrogen content was determined by SIMS at Charles Evans East. We have previously found good correlation between SIMS and FTIR. Experiments employing the photo-CVD reactor used techniques which did not require high substrate temperatures and are described in Section 2.2. This reduced the possibility of encountering problems when eventually incorporating these i-layers into a p-i-n device structure. In contrast, the low hydrogen work in the plasma-CVD reactor typically used substrate temperatures of 350°C, although films at 250°C were deposited as well, as described in Section 2.4.

Low hydrogen films in the photo-CVD system had adhesion problems with substrates of glass, metallized glass, or Si wafers. The flaking and peeling seemed worse on thicker films. This precluded measurements of optical properties, conductivity, or hydrogen by FTIR on most films. However, the films adhered very well to SnO_2 coated glass as used for device substrates. Therefore, evaluation of stability on photo-CVD materials shifted from film based to device based measurements using Schottky junctions. Specifically, changes in the short wavelength quantum efficiency (SWQE) with light exposure were used to characterize stability in low hydrogen photo-CVD materials. No adhesion problems occurred with plasma-CVD films. Section 2.4 contains results of a stability study comparing photoconductivity of photo-CVD and plasma-CVD films having 2-6% hydrogen.

2.2 GROWTH AND STABILITY OF LOW HYDROGEN PHOTO-CVD MATERIALS

Two different types of deposition conditions were investigated to reduce the hydrogen content of the photo-CVD films. One involved lower pressure (1 Torr) and lower UV light intensity (by 72%). The purpose was to reduce gas phase collisions leading to polymerization which is suspected as being a major source of

hydrogen in the film, especially dihydride bonding. Curiously, growth rate was relatively unaffected. The second type of growth condition which we investigated was to deposit film for a short interval (giving approximately 20Å of a-Si) then expose this recently grown layer to energetic Hg or H atoms. The purpose of the anneal or etch step is to scrub hydrogen atoms from the surface. The cycle of deposition and etching is repeated many times to obtain a film of sufficient thickness. This is comparable to the "chemical annealing" described by Asano (3). Table 1 lists deposition conditions of standard, light attenuated and chemically annealed films.

Due to the tendency of this film to flake and peel from glass or Si wafer substrates, the only useful substrate was textured SnO_2 (which we get from Solarex Thin Film Div.). A thin n-layer is deposited first to give an ohmic back contact, followed by the i-layer. Schottky junctions were formed at Penn State using semi-transparent Ni. Co-deposited samples were sent to Charles Evans for SIMS.

Table 2 shows the results of the SIMS study of photo-CVD materials from Table 1. Several of the results are mildly encouraging. The photo-CVD materials appear to have hydrogen contents lower than the industrial standard provided to us from Solarex. Also, the impurity contents are comparable to the industrial standard. However, our attempts to lower the hydrogen content by light attenuation and Hg annealing seem to have failed with the possible exception of sample #3492 for which the SIMS measurement indicates a low hydrogen content (this value is consistent with a concentration of ~2-3%). However, sample #3494 grown under similar conditions as #3492 had twice the hydrogen concentration. There are several possible explanations for this including a brief (5 minute) rise in chamber pressure during the deposition of #3494. However, no abrupt change in H, C, or O profile was seen on #3494. The accuracy of the SIMS technique could be responsible.

Table 3 shows the hydrogen content, SWQE in the annealed and degraded states ΔSWQE for four of the Schottky devices. Results of two p-i-n cells having 0.6 μm i-layers are also shown for purposes of discussion. We have previously discussed the deposition and stability of these devices, having 7 and 11% hydrogen (1,2). The device with 11% hydrogen (#3296) was found to have a much larger ΔSWQE, and poorer degraded performance compared to the standard device having 7% hydrogen content (3288).

Table 1

Growth conditions of low hydrogen photo-CVD films

Sample #	Comments	Cycle time (min.)	# of cycles	T_{dep} (°C)	Press. (torr)	--Gas Flow Rate-- (sccm) SiH_4	He	H
3482	72% light attenuated	400	1	250	1	2.8	2.8	0
3491	standard	335	1	205	5	2.0	8.0	0
3492	72% light attenuated	375	1	230	1	2.8	2.8	0
3493	standard	335	1	205	5	2.0	8.0	0
3494*	72% light attenuated	375	1	230	1	2.8	2.8	0
3496	1 min growth 2 min anneal	3	78	205	5	2.0	8.0	0
3497	1 min growth 5 min anneal	6	51	205	5	2.0	8.0	0
3505	2 min growth 0.5 min H etch	2.5	20	230	2/0.5	2.2	0	20
PB55	Solarex glow discharge	-	-	-	-	-	-	-

* pressure increased to 3 torr for ~ 5 minutes during run

Table 2

Thickness and SIMS analysis of low hydrogen photo-CVD films

Sample	d	Concentration ($X10^{21}cm^{-3}$) H	O	C	
3482	1.2	3.0	0.03	0.015	(more O and C at back)
3491	0.60	2.5	0.03	0.005	
3492	0.37	1.0	0.009	0.007	
3493	0.9	2.6	0.017	0.005	
3494	1.3	2.2	0.02	0.005	
3496	0.55	3.0	0.02	0.005	
3497	0.37	3.0	0.05	0.010	
3505	0.20	2-3	0.2-0.3	0.05	
PB55	-	4.0	0.009	0.010	

Table 3

SWQE stability measurements of low hydrogen photo-CVD Schottky and p-i-n cells. The i-layer of p-i-n 3288 was the same as that of 3491, our standard device i-layer.

Sample #	C_H(%)	Device	QE @ 450 nm Annealed	Degraded*	ΔSWQE
3491	5	Schottky	0.34	0.30	0.04
3492	2	Schottky	0.46	0.39	0.07
3496	6	Schottky	0.47	0.38	0.09
3497	6	Schottky	0.40	0.35	0.05
3288	6	p-i-n	0.57	0.41	0.16
3296	11	p-i-n	0.42	0.22	0.22

*Schottky devices degraded for 64 hours, p-i-n devices for 100 hours, both at 100 mW/cm^2.

There appears to be no correlation between ΔSWQE and hydrogen content of the Schottky devices. The SIMS value for H is likely to have a 10% uncertainty but this does not bring the results into any agreement. One possible complication is the difference in thickness (Table 2) since the ΔSWQE is known to be sensitive to i-layer thickness (1,2). However, cells 3292 and 3297 were the same thickness, yet the one with three times higher hydrogen had the lower ΔSWQE. This is in direct contrast to the p-i-n cells. Also, the two devices having standard i-layers of the same thickness (p-i-n #3288 and Schottky #3491) have dramatically different SWQE values (0.16 vs. 0.04). Different interfaces and window absorption are expected to influence the magnitude of the SWQE but it has been claimed (4) that the **change in SWQE** is an i-layer property reflecting the light-induced defect density of the i-layer. Data from Schottky and p-i-n devices are jointly presented in reference 4. Yet, the data of Table 3 clearly indicates that the ΔSWQE does not represent an unambiguous i-layer property but depends on device structure.

A p-i-n device (#3507) was deposited with light attenuated i-layer conditions as used for 3492 and 3494 (Table 1). Voltage dependent QE measurements indicated a good p/i interface but poor hole collection. Cells had very poor FF (48-50%) and larger light-dark crossover. Stability was not evaluated because of the poor initial performance (η~5%).

The stability data of Table 3 does not allow us to draw any conclusion about the stability of low hydrogen photo-CVD films fabricated into Schottky junctions. (Discussion and results of stability of photo-CVD films based on photoconductivity is presented in Section 2.3). We feel confident in repeating the conclusion of ref. 1 and 2 based on the p-i-n devices 3288 and 3296 that photo-CVD material with 7% hydrogen is more stable than material with 11% hydrogen. In that study there was at least some correlation between the magnitude of the SWQE and measured cell performance. Uniform devices (same i-layer thickness and cell structure), a clear link between the ΔSWQE and i-layer quality, and reproducible H content are needed to further study the effect of low hydrogen content on device stability. The SWQE technique is not a clear measure of i-layer quality and should not be used without further experimental and theoretical verification.

2.3 GLOW DISCHARGE MICROCRYSTALLINE FILMS

Compared to the photo-CVD deposition system, the chemistry of glow discharge deposition is less well understood. While the deposition and etching species in the glow discharge system are related to the composition and structure of the growing film as they are in photo-CVD, it is not possible to rely on a mathematical model to predict the fluxes of these species. In

glow discharge deposition we are presently limited to experimental data from which relative fluxes can be inferred. For example, from our photo-CVD work we know that the onset of microcrystalline growth begins when the hydrogen radical flux is comparable to the silicon radical flux. Therefore, one of the deposition conditions that was of particular importance was the growth conditions for microcrystalline films since this can be used to establish that a significant hydrogen radical flux rate is present during deposition.

Films were deposited in the glow discharge reactor as a function of hydrogen dilution. The range of deposition parameters was chosen to be large enough to include the deposition of amorphous and microcrystalline films. The absorption coefficient versus wavelength for a number of films is shown in Figure 1. Note that some of the doped microcrystalline films absorb light as strongly as amorphous films, a fact that may reduce the utility of microcrystalline films in multi-junction tunnel junctions. Shown in Figure 2 is an X-ray diffraction scan of an undoped silicon film where the sharp peak indicates the presence of crystalline structure. However, the broad feature around 25 cm^{-1} indicates a significant amount of amorphous material.

Electrical and optical properties of a-doped a-Si n-layer, doped μc-Si n-layer, and undoped μc-Si layer are given in Table 4. The absorption coefficients were shown in Fig. 1. The μc-Si film (4021) has low conductivity and large activation energy despite clear evidence of its microcrystallinity from XRD in Fig. 2. Phosphorous doping dramatically increased the conductivity (4027). Similarly, the transition from amorphous to microcrystalline between 4025 and 4027 occurred with a small increase in RF power. This is consistent with reports of the extreme sensitivity to deposition conditions of the on-set of microcrystallinity.

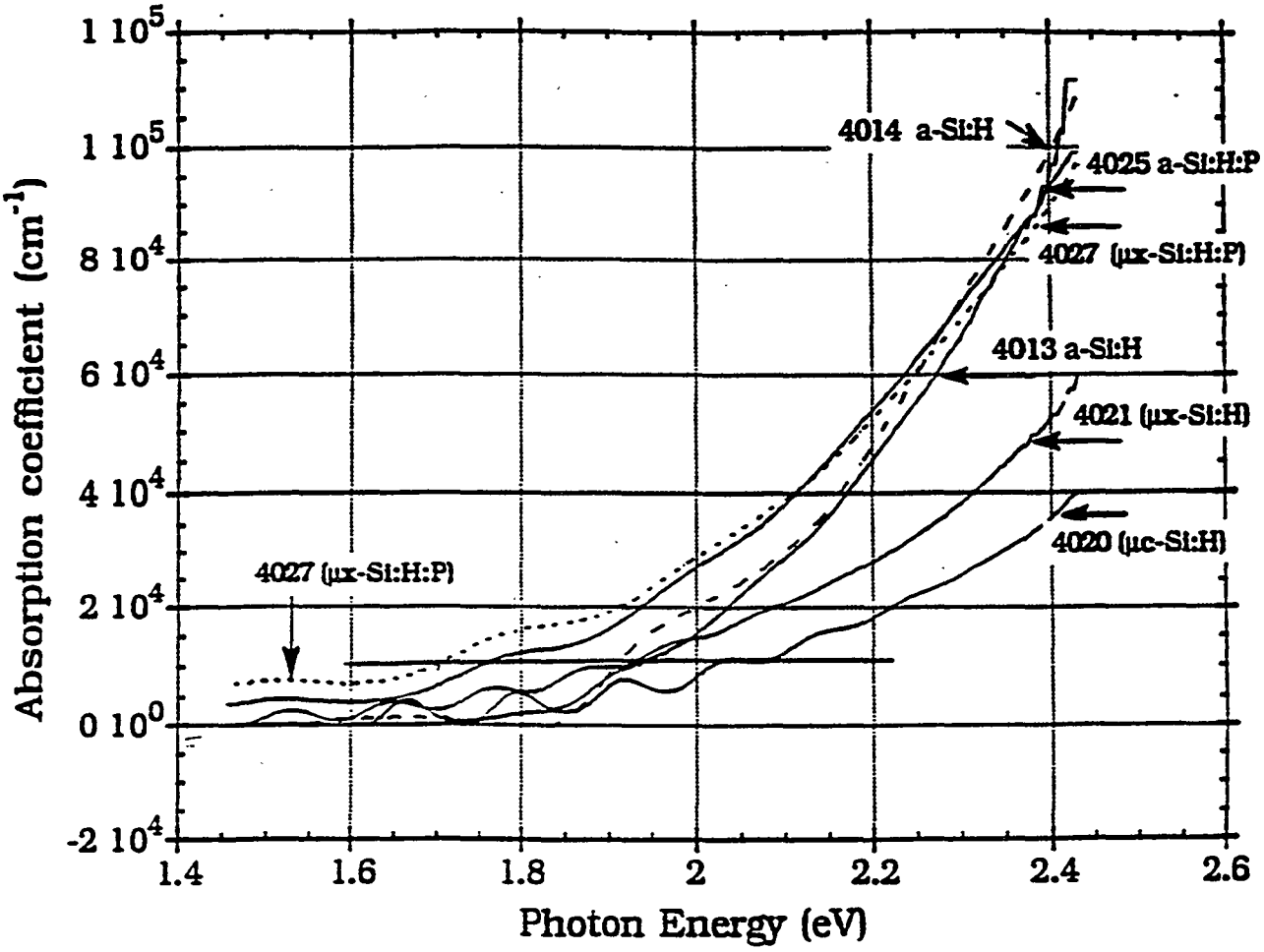

Figure 1 The absorption coefficient versus wavelengths for a number of films grown by RF glow discharge.

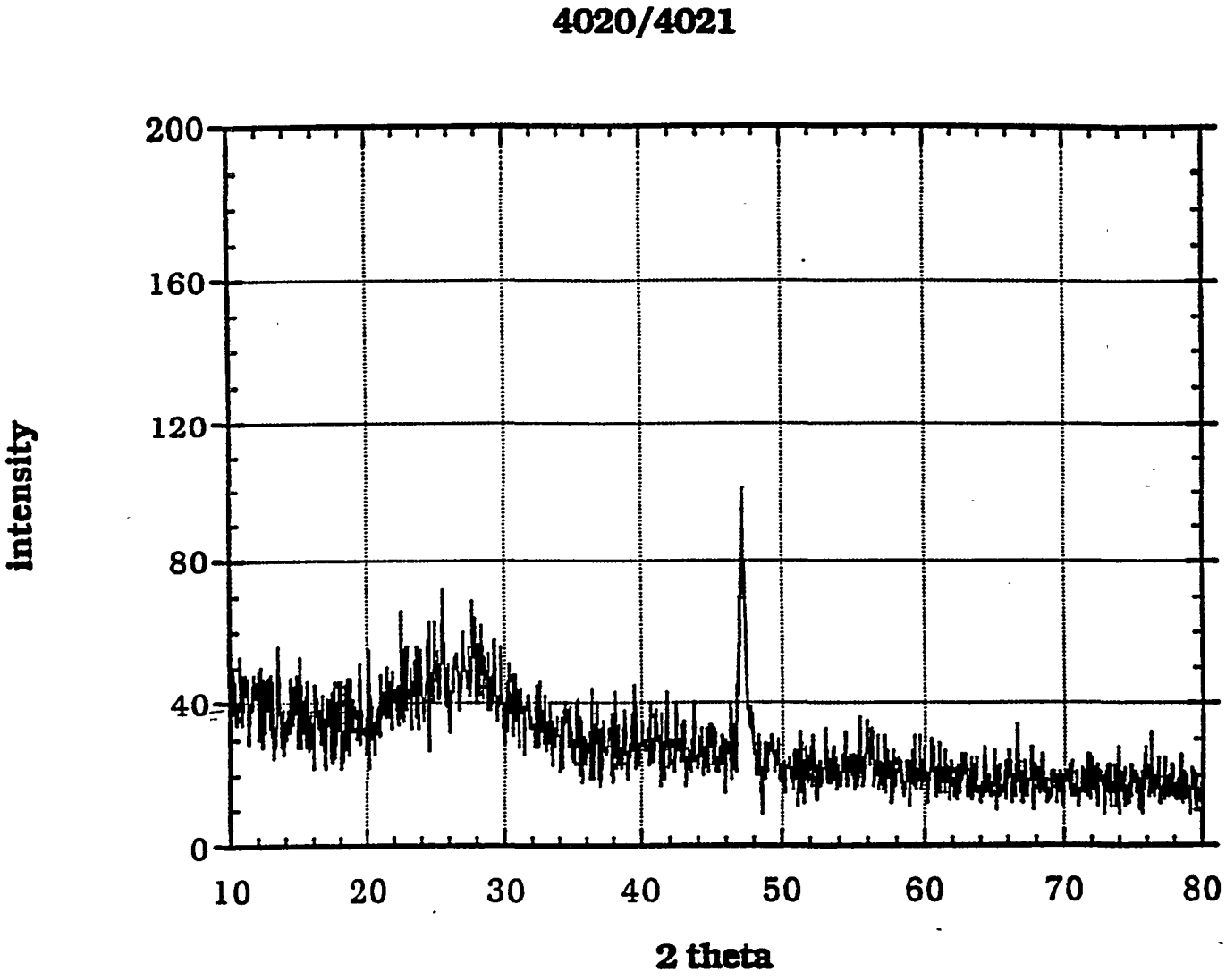

Figure 2 The X-ray scan of a microcrystalline film grown by RF glow discharge.

Table 4. Properties of amorphous and microcrystalline layers

Film	PH_3 doped	Deposition Temperature	Power (W)	E_{04} (eV)	σ_D (S/cm)	E_A (eV)
4025(a-Si)	Yes	250°	55	1.72	2E-4	0.32
4021(μc-Si)	No	330°	77	1.92	9E-4	0.31
4027(μc-Si)	Yes	250°	67	1.70	3	<0.05

2.4 LOW HYDROGEN FILMS GROWN BY GLOW DISCHARGE

During this phase of our research our glow discharge reactor became fully operationable. To confirm the material quality of the glow discharge reactor, several solar cells were prepared. Even though doped and buffer layer recipes were not optimized, a solar cell of 8% efficiency was prepared after only three attempts. No further solar cell work was conducted in the glow discharge reactor.

A-Si:H films were deposited in the plasma reactor under conditions of high substrate temperature (350°C) and hydrogen dilution. It was expected that low hydrogen content would result. The total flow, power and pressure were fixed (30 sccm, 9.6W and 0.5 Torr, respectively). Films on Si wafers were sent to Charles Evans for SIMS determination of H content. Photoconductivity, dark conductivity, and activation energy were measured at IEC on gap samples. Flow rates, thickness, and film results are given in Table 5. Note that the hydrogen content is below 5% on all films, including 4065 deposited without any hydrogen dilution (straight SiH_4). This suggests that the high substrate temperature is the more important factor in reducing hydrogen. The impurity concentration of C and O are comparable to the photo-CVD films in Table 2. The C is 3-5X lower than the Solarex sample. It is recognized that depositing p-i-n devices with i-layers at 350°C is problematic.

Eight a-Si films having low hydrogen content (2-6%) were exposed to 200 hours of light (100 mW/cm^2, ELH, 25°C). Six were deposited by glow discharge (Table 5) and two were typical device i-layers by photo-CVD. Photoconductivity was measured at periodic intervals. The film deposition method, substrate temperature, growth rate, hydrogen content and initial and final photoconductivity are given in Table 6. Note that substrate temperatures ranged from 205 to 350°C and growth rates from 1 to 9 Å/s. Figure 3 shows the time dependence of the photoconductivity of 4 films, covering the range of temperature, deposition method, and hydrogen content from Table 6. Yet, there was little difference in either the rate of degradation or the final value. The photoconductivity degraded typically by a factor of five from the initial value. This is smaller than what

Table 5. Deposition conditions and film properties of low hydrogen a-Si:H films deposited in plasma reactor. Total flow=30 sccm, temperature=350°C, pressure=0.5 Torr, and power=9.6 W.

Film	H_2/SiH_4 (sccm)	Growth rate (Å/s)	Thick. (μm)	SIMS(x10^{21}cc) C	O	H	%H	photo (S/cm)	dark (S/cm)	E_a (eV)
4061	24/6	1.5	0.54	.006	.05	1.4	2.8	1.0E-4	2.4E-8	0.57
4062	6/24	7.3	0.66	.003	.03	1.2	2.4	1.9E-4	8.6E-9	0.63
4063	12/18	2.9	0.35	.003	.03	1.8	3.6	9.5E-6	6.2E-10	0.70
4064	18/12	3.3	0.59	.002	.02	1.9	4.0	9.8E-6	2.2E-9	0.67
4065	0/30	9.4	1.7	.001	.007	1.6	3.1	2.1E-5	5.2E-10	0.75
4015*		1.4	0.51	.002	.02	2.0	4.0	2.1E-5	3E-11	0.80

*deposited at 250°C

Table 6

Photoconductivity before and after 200 hrs light soaking for low hydrogen content amorphous silicon films

Film #	Deposition Method	Substrate Temperature (oC)	Growth Rate (Å/sec)	Hydrogen Content (%)	Photoconductivity (μS/cm) Initial	Final
4061	plasma	350	1.5	2.8	88	7.5
4062	plasma	350	7.3	2.4	21	4.8
4063	plasma	350	2.9	3.6	16	4.7
4064	plasma	350	3.3	4.0	11	4.1
4065	plasma	350	9.4	3.1	20	3.4
4015	plasma	250	1.4	4.0	21	3.5
3098	photo	205	2.0	5.4	18	4.6
3323	photo	205	0.9	6.1	34	6.5

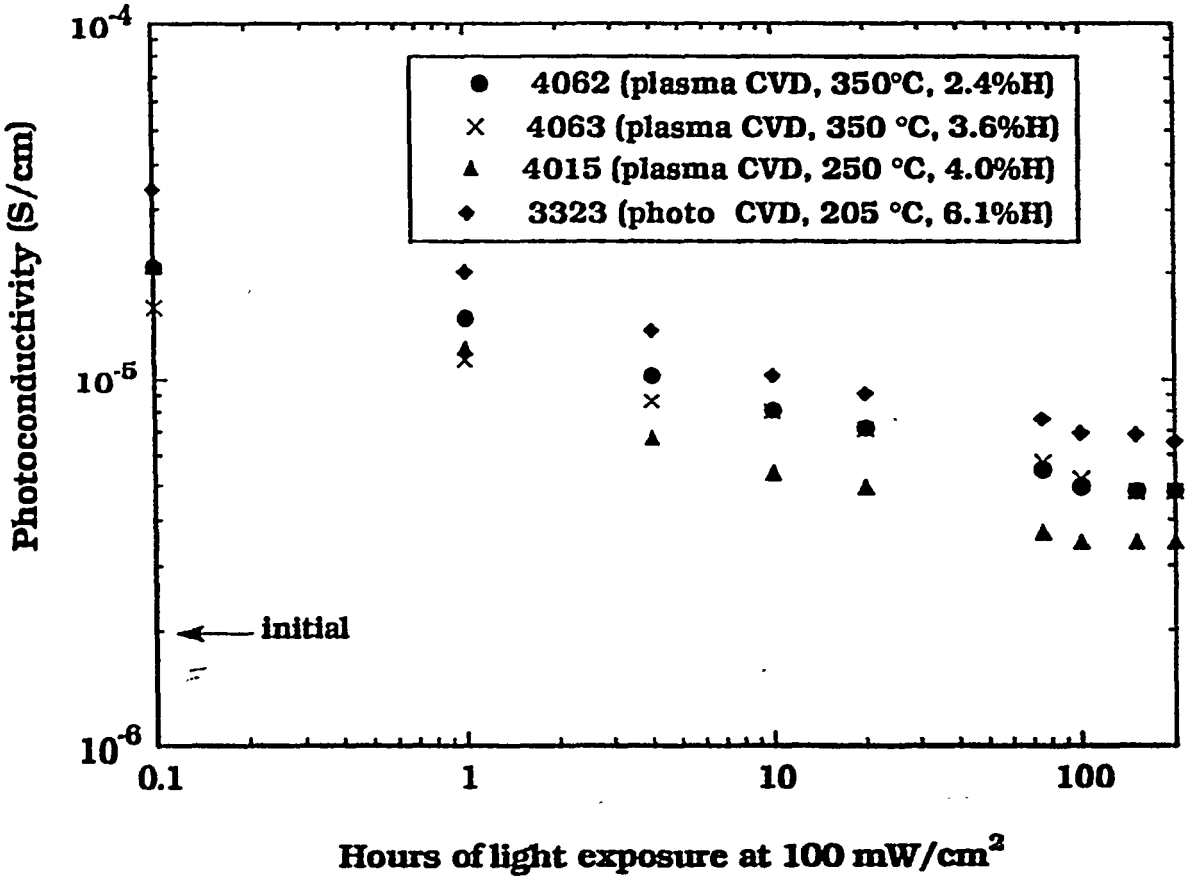

Figure 3 Change in photoconductivity during 200 hour light exposure films having H~2-6% (Deposition temperature and %H given).

is typically reported for higher hydrogen films, which may degrade by a factor of 10 or more with only 20 hours light soaking (ref. 5-7). The photoconductivity for all four films tends toward saturation after 100 hours at values which are within a factor of two of each other. Figure 4 clearly shows that the final value is independent of hydrogen content.

These results are significant since they show that films having low hydrogen content (<8%) are more stable than films having higher hydrogen. However, there does not seem to be a difference in stability once the hydrogen content is in the 2-6% range.

This is in contrast to some results (6) but in agreement with others (7). We acknowledge that photoconductivity may not be the most sensitive measure of light induced defects. The low hydrogen films were obtained at different substrate temperatures, growth rates, and deposition methods, yet these made no significant difference to the degradation. Finally, we note that at least one of the plasma CVD films (#4015, 4% H) was deposited at temperatures which are device-friendly (250°C) as opposed to the very high temperatures used by some groups to lower hydrogen (350-450°C, ref. 3).

2.5 THERMODYNAMIC DESCRIPTION OF THE STAEBLER-WRONSKI EFFECT

A thermodynamic description of the Staebler-Wronski effect was developed in collaboration with Penn State University and the University of Oregon (8,9). Although a negative change in entropy results from the application of thermodynamic equilibrium, it would be unreasonable to attribute such entropic changes to electronic transitions alone since the magnitude is closer to values involved with phase change. Since the thermodynamic description does not a-priori attribute the energetic changes to electronic levels either, it is also reasonable to assume that some of the free energy changes of dangling bond formation are related to lattice relaxations. In this view the loss in energy and the loss in entropy are those of the lattice moving towards a more ordered 'crystalline-like state'. Considering structural changes only, the lowest energy state for the dangling bond-lattice system is with the weak bonds split into neutral and charged dangling bonds.

One practical result of this work is the establishment of a theoretical framework which supports the observation that solar cell efficiencies tend to stabilize during field testing. This is explained by applying the high temperature equilibrium behavior to solar cells at normal operating temperature and illumination level. Unlike other Staebler-Wronski descriptions, the thermodynamic description predicts that a saturation of the dangling bond concentration occurs at levels below the total weak bond density. The saturation level is expected to be a function

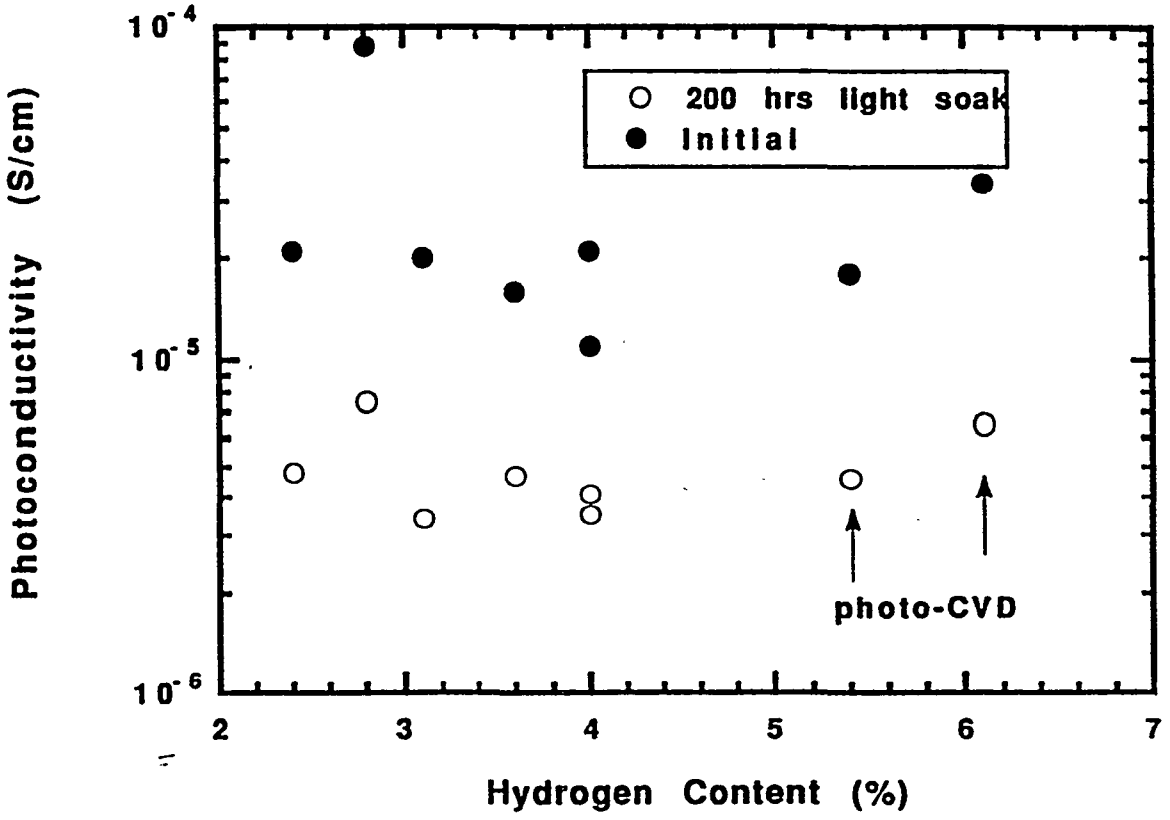

Figure 4 Initial and final photoconductivity of 8 films having H~2-6%. Data from Table 6. Deposition by plasma-CVD unless noted.

of the illumination intensity and the operating temperature. The expected saturated defect concentration is important for the comparison of various materials and to obtain parameters for modeling designed to improve the stabilized solar efficiency.

2.6 COMPARISON OF FAST AND SLOW DEGRADATION

Accelerated light soaking has been investigated by a number of groups. In order to determine if we could use accelerated degradation, a collaboration with the University of Neuchatel was undertaken to compare fast (accelerated) light soaking at high light intensities (50 suns) and the more standard (slow) degradation that occurs at operating solar cell illumination levels (1 sun).

The effect of room temperature dark annealing of device degradation initially noted by the University of Neuchatel was also examined. The literature has also reported but does not explain the reduction of defect concentrations under low current injection in the dark. Our results show that only defects created by fast, high intensity degradation anneal at room temperature in the dark.

It is important to note that the fill factor is a poor measure of absolute defect densities in general since an exact relationship is not known. However, the fill factor (or efficiency) can be used to establish the rate of change of defect densities if precautions are taken. To establish the rate of change of defects, it is only necessary to assume that the relationship between the defect density and the fill factor is one-to-one and monotonic. Because of the complex relationship between dangling bonds and fill factor one must always take the precaution of choosing a constant value of the fill factor at which to measure the rates of change. With this precaution it becomes unnecessary to know the relationship between absolute dangling bond concentrations and fill factor. We can then write the following relation between the rates of FF and N_{DB} as:

$$d(FF)/dt=(d(FF)/dN_{DB})*(dN_{DB}/dt) \quad (1)$$

If one compares similar solar cells (i-layer thickness, deposition conditions, etc.) and care is taken to compare solar cells of the same fill factor (or efficiency), the first derivative on the right hand side of equation 1 is constant. Therefore, the rate of change in fill factor is approximately proportional to the rate of change of defect densities. Figure 5 shows the fill factor as a function of time in the dark at room temperature for two co-deposited samples following different degradation methods. One sample was light soaked for 2000 hours at approximately one sun illumination. The FF of this cell showed a negligible room temperature relaxation rate. In contrast a cell which was brought quickly to the same degraded

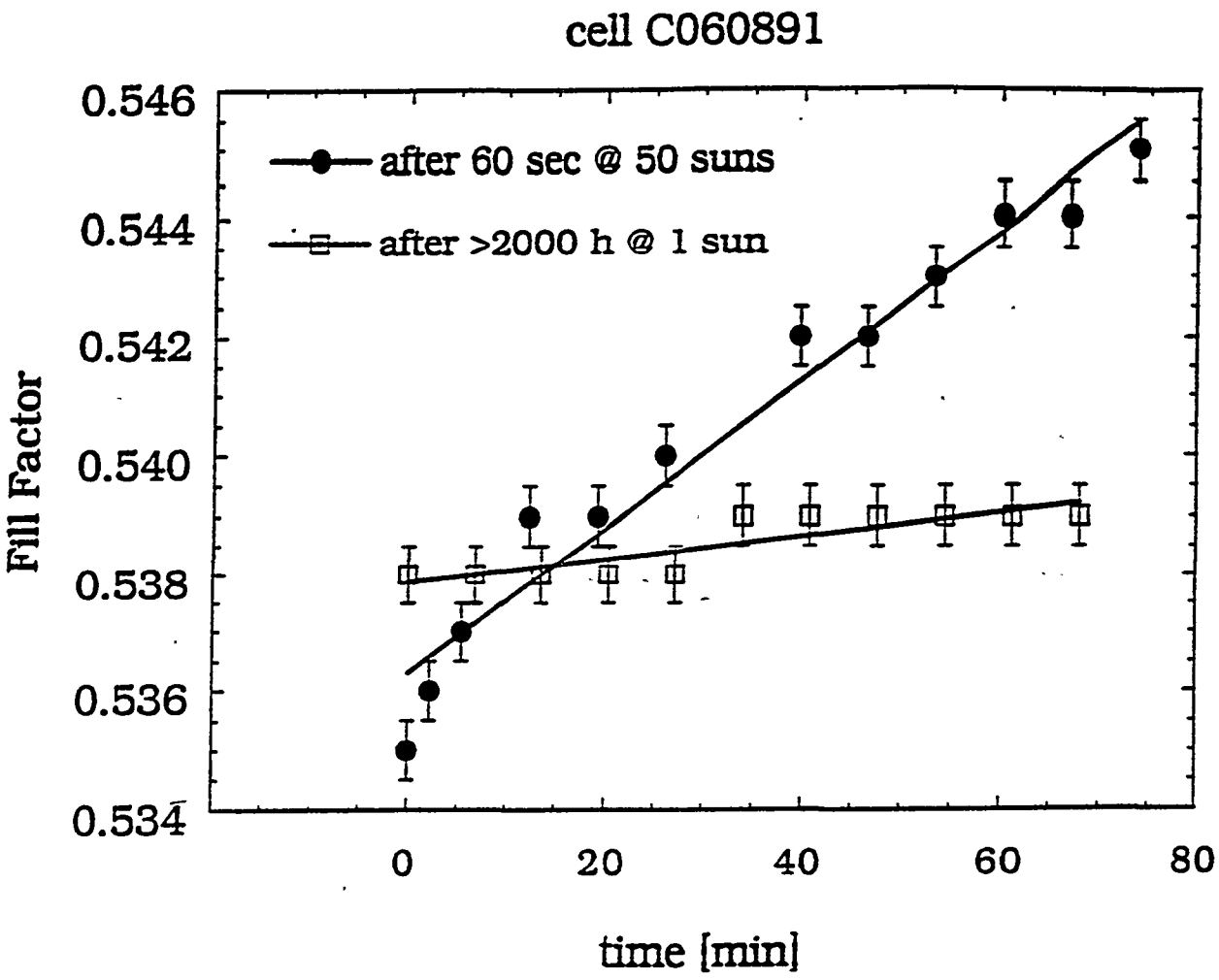

Figure 5 Dark recovery of FF following slow and rapid degradation (low and high intensity light soaking).

state by high intensity laser light showed a large relaxation rate. The fill factor markedly improved in the dark after the illumination was turned off. Since both samples were degraded to approximately the same fill factor (the first term on the right hand side of equation 1 is the same for the two cases) we are justified in assuming the rates of recovery are directly proportional to the differences in the rates at which dangling bond defects are eliminated by relaxation in the two samples. Because of the difference between quickly degraded and slowly degraded fill factor relaxation rates (and hence the defect density relaxation rate), it is not possible to view fast and standard degradation as equivalent. Since the behavior of Neuchatel (VHF GD) and IEC (photo-CVD) samples is similar, this is probably representative of amorphous materials. If an extrapolation is made to other accelerated degradation techniques, a dark reduction of defect densities would be expected. This could explain most relaxation phenomena including the reduction of defect densities due to high density current injection (10).

We are presently examining the concept that, unlike standard degradation, the accelerated degradation does not allow sufficient time for the lattice relaxation as suggested by the thermodynamic description. A failure of the lattice to fully relax would permit a larger than equilibrium concentration of defects to be formed, since, the formation of defects is driven by energetics involving lattice relaxation.

SECTION 3.0

TASK 2 - a-SiGe:H MATERIALS AND DEVICES

A number of a-SiGe films were grown by photo-CVD at IEC for detailed characterization at other laboratories since our own capabilities are limited to basic properties such as conductivity and bandgap. Preparation of these specialized samples was often quite difficult, requiring 6-8 hour depositions and specialized substrate handling. Results of these collaborative efforts are described in Section 3.1. Characterization of hole and electron collection and stability of graded a-SiGe p-i-n cells is found in Section 3.2. Results from film and device measurements are compared and discussed in Section 3.3. Sections 3.4 and 3.5 describe modelling of a-SiGe single and multijunction devices.

3.1 a-SiGe FILM CHARACTERIZATION AND ANALYSIS

3.1.1 Optical Characterization

A series of a-SiGe films were prepared with thicknesses from 0.02 to 0.6 μm for optical absorption analysis at Penn State University. The absorption spectra, shown in Figure 6, was obtained from different methods in different regions (11). The films were deposited under conditions (230°C, 5 Torr, $SiH_4/GeH_2/H_2$=11.5, 1.5, 50 sccm) which we have used for most of our a-SiGe devices. We consider this to be our standard a-SiGe material. Films deposited under these conditions in the past have consistently had Ge content of 62(+/-3)% and bandgaps of 1.30 (+/-0.03 eV). However, the absorption data of Figure 6 yields a bandgap of 1.43 eV as shown in the Tauc's plot of Figure 7. This corresponds to a Ge content of about 45% in the film. The parameter E_{04} from Figure 6 is 1.56 eV suggesting a Tauc's bandgap of 1.40-1.45 eV. Lower-than-expected Ge content was confirmed by measurements on a series of films which we provided to Univ. of Oregon, discussed in the next section. Film 3481, deposited under the same conditions as 3534, was found to have only 47% Ge instead of the 60% expected. These results indicate that the relation between a-SiGe deposition conditions and resulting film composition needs to be re-evaluated.

The Urbach energy from Figure 6 is 59 meV which is slightly larger than found by others for this bandgap. We have found values of 46-50 meV (12,13). The midgap absorption was similar to that reported by others for alloys of similar bandgap. Values of α=3-10 cm^{-1} at 0.8 eV are commonly observed for alloys with bandgaps of 1.3-1.4 eV. Comparison to the midgap absorption of a-Si suggests the defect density causing the absorption has increased by 10-30X with alloying. After 100 hours of light soaking at 100 mW/cm^2, Figure 6 shows negligible increase in deep defects, suggesting much better stability than a-Si. These results will be compared to other measurements in Section 3.3.

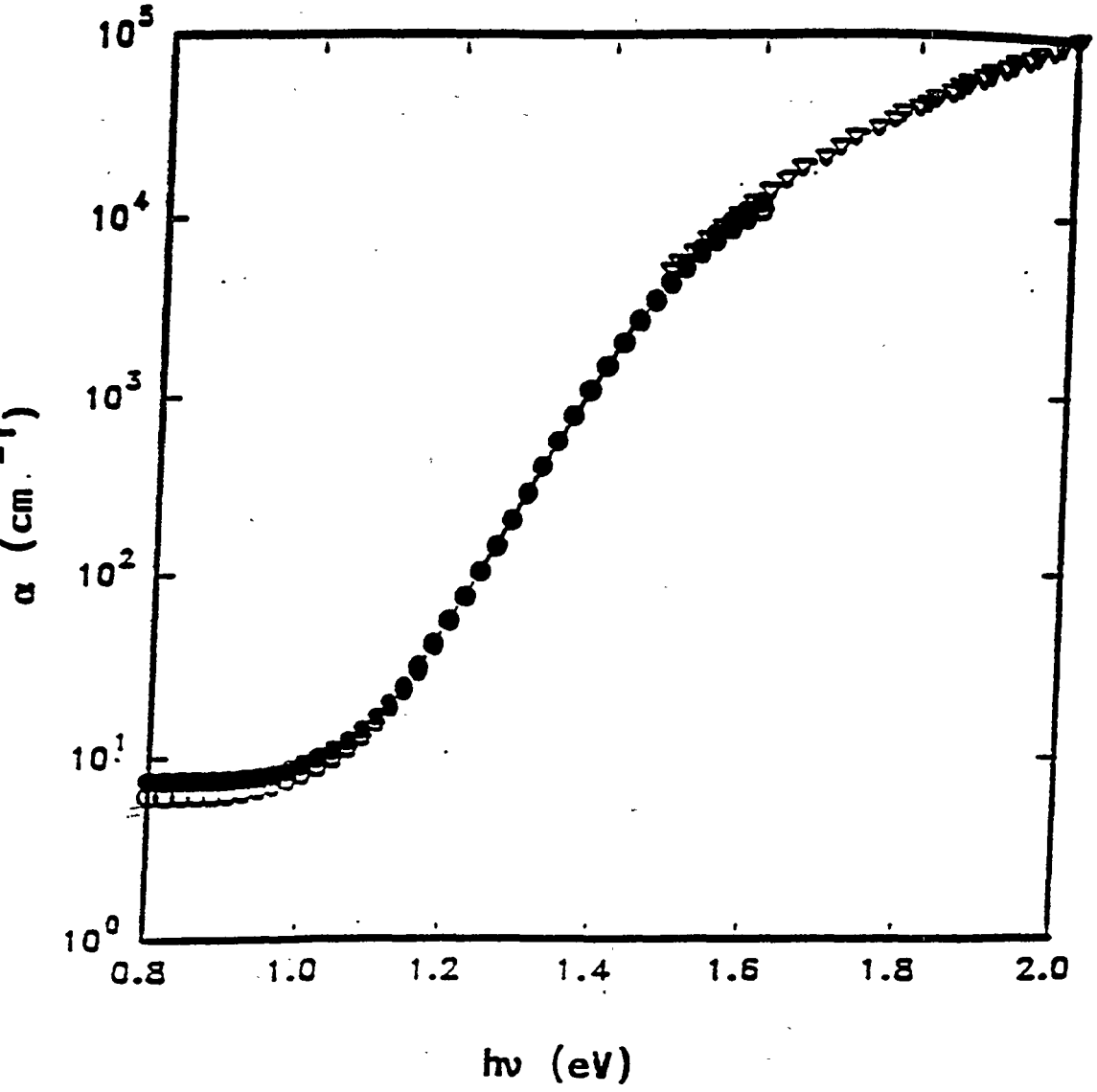

Figure 6. Absorption coefficient of a-SiGe film. Open circles are initial, closed circles are after 100 hours light soaking.

3.1.2 Steady-state Electron and Hole Transport

The photoconductivity, quasi-Fermi level, and electron $\mu\tau$ for the same a-SiGe film whose absorption is given in Figures 6 and 7 (0.6 μm thick, 1.43 eV) is listed in Table 7. The data was obtained by dual beam photoconductivity (DBPC) over four orders of magnitude at Penn State. A value of γ=0.6 was obtained from the intensity dependence. Extrapolating to 1 sun generation rates ($5x10^{20}/cm^3s$) gives a $\mu\tau$ of less than $1x10^{-7}cm^2/V$-s which is 10-50 times lower than found for device quality a-Si. We have previously shown (1) that the hole $\mu\tau$ from SSPG is $1-2x10^{-9}cm^2/V$ for our low bandgap a-SiGe films. Thus, the hole $\mu\tau$ is over an order of magnitude smaller than the electron $\mu\tau$ at 1 sun intensity. Based on these material transport properties, the hole is expected to be the limiting carrier in low bandgap solar cell performance.

3.1.3 Capacitance and Transient Photocharge Methods

Drive-level capacitance and sub bandgap transient photocharge methods were used to characterize our films at University of Oregon in collaboration with J.D. Cohen. Initial results have been published (14) on materials spanning the alloy system. (The Ge contents listed in that paper have since been found to be in error. They were initially estimated from deposition conditions but have recently been measured at NREL by microprobe.) Results of Urbach and Fermi energies, defect density, and deep trapping hole $\mu\tau$ are given in Table 8. The latter two properties were measured in initial and light soaked states (A and B). The a-SiGe films were all deposited at 230°C, 5T, with H dilution. Note that 3481 and 3420 were deposited with identical gas flows yet Ge contents of 47 and 58% resulted, consistent with the large difference in film properties. Films with higher Ge content were also supplied but defect densities were too high for meaningful evaluation.

The Urbach energy is essentially unchanged with Ge up to 47%. The defect density in state A increases by only a factor of 5 with the addition of 47% Ge but then quite steeply (factor of 25) in the 58% Ge alloy, compared to a-Si. There is a corresponding sharp increase in the Urbach energy and sharp decrease in hole $\mu\tau$ between these two concentrations. Since these two films were intended to be deposited under the same conditions, we suspect that the gas flows were different leading to higher Ge incorporation for 3420. This is consistent with some variability observed in device results. Since the a-SiGe layers in our devices are made with the same recipe used to deposit these two films (3481 and 3420) it can only be said that the defect density of the a-SiGe device layers is 5-25 times higher than for the a-Si device layers.

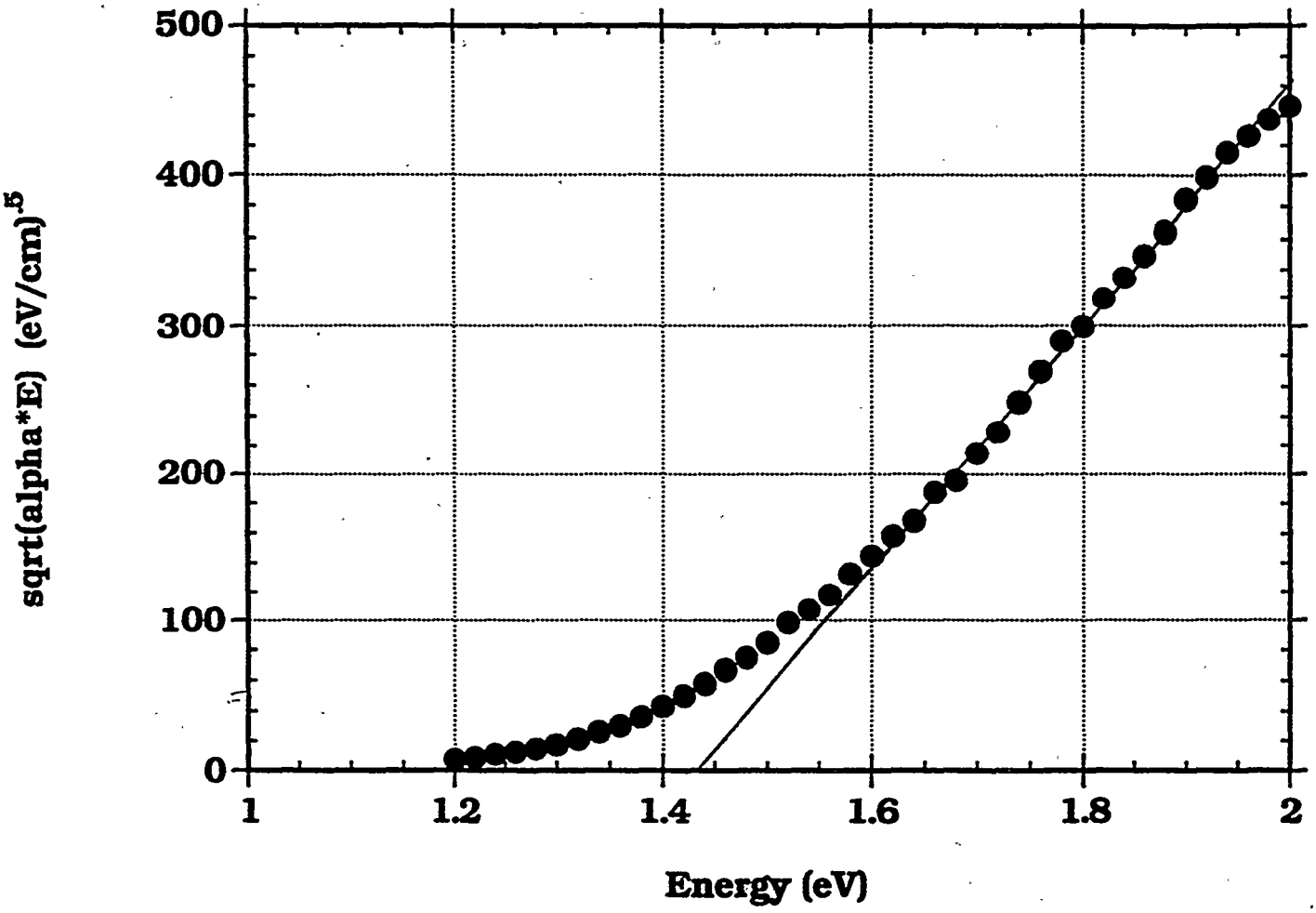

Figure 7. Tauc's plot of absorption data of Figure 6 giving a bandgap of 1.42 eV.

Table 7

Photoconductivity intensity dependence for a-SiGe film #3534 measured by DBPC at Penn State

Sample#	E_g(eV)	d(μm)	G(cm^{-3}/s)	σ_p(ohm-cm)$^{-1}$	E_c-E_{fn}(eV)	$\mu\tau$(cm^2/V-s)
3534	1.42	0.60	2.38E19	8.15E-7	0.534	2.14E-7
			2.38E18	1.89E-7	0.572	4.95E-7
			2.76E17	5.31E-8	0.605	1.20E-6
			2.88E16	1.43E-8	0.638	3.10E-6
			3.34E15	4.05E-9	0.671	7.58E-6

Table 8

Optoelectronic properties of series of a-SiGe films deposited by photo-CVD at 230°C, 5T. Measurements performed at Univ. of Oregon. State A=annealed, state B=50 hrs exposure to 400 mW/cm^2 of filtered light (except a-Si sample which received 100 hrs).

Ge= %Ge in film from microprobe at NREL
E_A= activation energy from capacitance turn-on
E_U= Urbach energy from transient photocurrent
N_D= deep defects near E_A from drive level capacitance
$\mu\tau_p$= deep trapping product for holes (not same as recombination-limited $\mu\tau$) from analysis of transient photocurrent and photocapacitance

Film #	Ge %	E_A (eV)	E_U (meV)	N_D (cm-3) A	B	$\mu\tau_p$(cm^2/V) A	B
a-Si	0	0.70	48	4E15	3E16	6E-9	6E-10
3539	29	0.65	50	6E15*	1E16	1E-9	4E-10
3512	37	0.69	51	8E15	3E16	3E-9	6E-10
3511	42	0.61	51	1E16	4E16	1E-9	3E-10
3481	47	0.57	52	2E16	6E16	7E-10	8E-11
3420	58	0.52	57	1E17*	-	3E-11	-
3442	100	0.45	50	9E17	-	-	-

*spin density on these films measured by ESR

The deep trapping hole $\mu\tau$ products decrease significantly with Ge content, as reported by others. Light soaking increases the defect density by 2-3 for all alloys, yet the hole $\mu\tau$ decreases by a factor of 4-9. The steady state hole $\mu\tau$ is relatively less sensitive to alloying or light soaking, as discussed in Section 3.3.

Comparison of spin density by ESR to defect density by capacitance can identify the presence of charged defects since ESR detects only neutral (singly occupied) states and capacitance detects all states containing charge (14). As discussed in ref. 14, charged defects may be present in the low Ge content film (3539) but not in the high Ge content, high defect density film (3420).

3.2 a-SiGe SOLAR CELL PERFORMANCE AND STABILITY

3.2.1 Background and Experimental Methods

The generally observed deterioration of material properties and device performance with incorporation of Ge can be somewhat overcome by bandgap grading (15-17). It is well established that grading the bandgap from low value (1.3-1.5 eV) near the p-layer to a high value (i.e. 1.75 eV a-Si) at the n-layer improves the initial and stabilized performance compared to ungraded or opposite graded cells. Various explanations for the improvements have been given, including improvements in hole collection (15,16) or electron mobility gradients (17). We have studied simplified versions of the continuously graded devices used by others, consisting of abruptly graded a-SiGe/a-Si i-layers. The stability of bifacial devices, having transparent front and back contacts, for bifacial photocurrent measurements was characterized. This allows probing electron (hole) limited collection using strongly absorbed blue light through the p(n) layer (16-18). Both steady state current voltage (J(V)) and chopped photocurrent voltage (QE(V)) behavior is reported on bifacial a-SiGe:H p-i-n devices.

Devices were deposited by photo-CVD as previously described with a 100 Å a-Si buffer layer between the a-SiC p-layer and the a-SiGe i-layer. All devices were either front-loaded with the low bandgap material nearer the p-layer than the n-layer [p/(500Å of a-SiGe)/(500Å of a-Si)/n] or ungraded (1000Å of a-SiGe). They were completed with ITO (transparent) or ITO/Ag (standard reflective) back contacts. Cells were light soaked through the p-layer for 200 hours with ELH lights at 100 mW/cm^2 at 25°C. Performance was measured with standard AM1.5 illumination, as well as red (630 nm long pass filter) and blue (550 nm short pass filter) light. Voltage dependent photocurrent response was measured with chopped light at 450 nm (strongly absorbed) and 750 nm (weakly absorbed).

3.2.2 Characterization of Effect of Grading and Bandgap Using Bifacial a-SiGe Solar Cells

Front loaded solar cells having 500Å of 1.4 eV a-SiGe produced 6.0% initial efficiency. The QE at 800 nm was 0.25 indicating good collection of red light. Table 9 lists the performance during 265 hours of light exposure. After the first 12 hours, the FF remains fairly constant (53-54%). Some of the losses may be related to scratching the contact due to repeated testing. Figure 8 shows the voltage bias dependence of the QE as the ratio of QE(-1V)/QE(0V). The progressive increase in the bias dependence is greater at short wavelengths than at long wavelengths, suggesting that the electron collection degrades more than the hole collection.

The effect of a-SiGe bandgap in abruptly graded devices was examined using bifacial measurements. Table 10 lists the initial performance of three front loaded devices, having 500Å of a-SiGe with estimated bandgaps of 1.5, 1.4, and 1.3 eV. V_{oc} and FF decrease with decreasing bandgap. The FF for blue light through the n-layer is always greater than for blue light through the p-layer. The opposite is found for ungraded (Table 11) or back loaded devices (17). This indicates that hole collection, i.e. the limiting carrier for strongly absorbed light through the n-layer, is improved more than electron collection in the front loaded device. This agrees with conclusions of others (15,16) and with the improvement in device performance with B doping of the i-layer (19). This contradicts previous claims (17) that front loaded devices had improved electron mobility through mobility gradients. As discussed in Section 3.1.2, the steady state electron $\mu\tau$ is ten times greater than the hole $\mu\tau$ in our standard 1.4 eV a-SiGe at 1 sun intensity, verifying that holes are the limiting carrier for n-layer illumination. Note that V_{oc} is approximately the same for illumination through the p or n-layer for both types of illumination. This implies that the V_{oc}-limiting recombination is not strongly dominated by one interface.

Table 9

Performance of cell 3520-11-1 (graded a-SiGe) during light exposure at 100 mW/cm^2, 25°.

Date	Condition	V_{oc} (V)	J_{sc} (mA/cm^2)	FF (%)	η (%)
11/11/91	init. test	.605	16.85	58.5	6.0
1/29/92	15min/160°C	.614	16.94	57.0	5.9
1/30/92	12 hrs	.585	16.5	53.9	5.2
2/4/92	100 hrs	.579	16.2	54.1	5.1
2/7/92	retest	.582	16.3	54.4	5.2
2/10/92	169 hrs	.565	16.2	53.0	4.9
2/17/92	265 hrs	.574	16.0	53.4	4.9

Table 10

Performance of front loaded a-SiGe/a-Si devices for two types of illumination through the p and n-layers. All i-layers were 500Å a-SiGe/500Å a-Si.

Device E_G	Illumination through	type	V_{oc} (V)	J_{sc} (mA/cm^2)	FF (%)
3528	p	AM1.5	.63	11.4	49.5
(1.5 eV)		blue	.61	4.2	**46.9**
	n	AM1.5	.65	10.9	55.9
		blue	.60	3.8	**61.5**
3548	p	AM1.5	.60	14.8	48.3
(1.4 eV)		blue	.57	5.4	**51.0**
	n	AM1.5	.59	14.0	52.2
		blue	.56	4.9	**55.3**
3527	p	AM1.5	.57	14.0	34.4
(1.3 eV)		blue	.50	5.5	**36.8**
	n	AM1.5	.55	14.4	39.3
		blue	.51	5.4	**42.3**

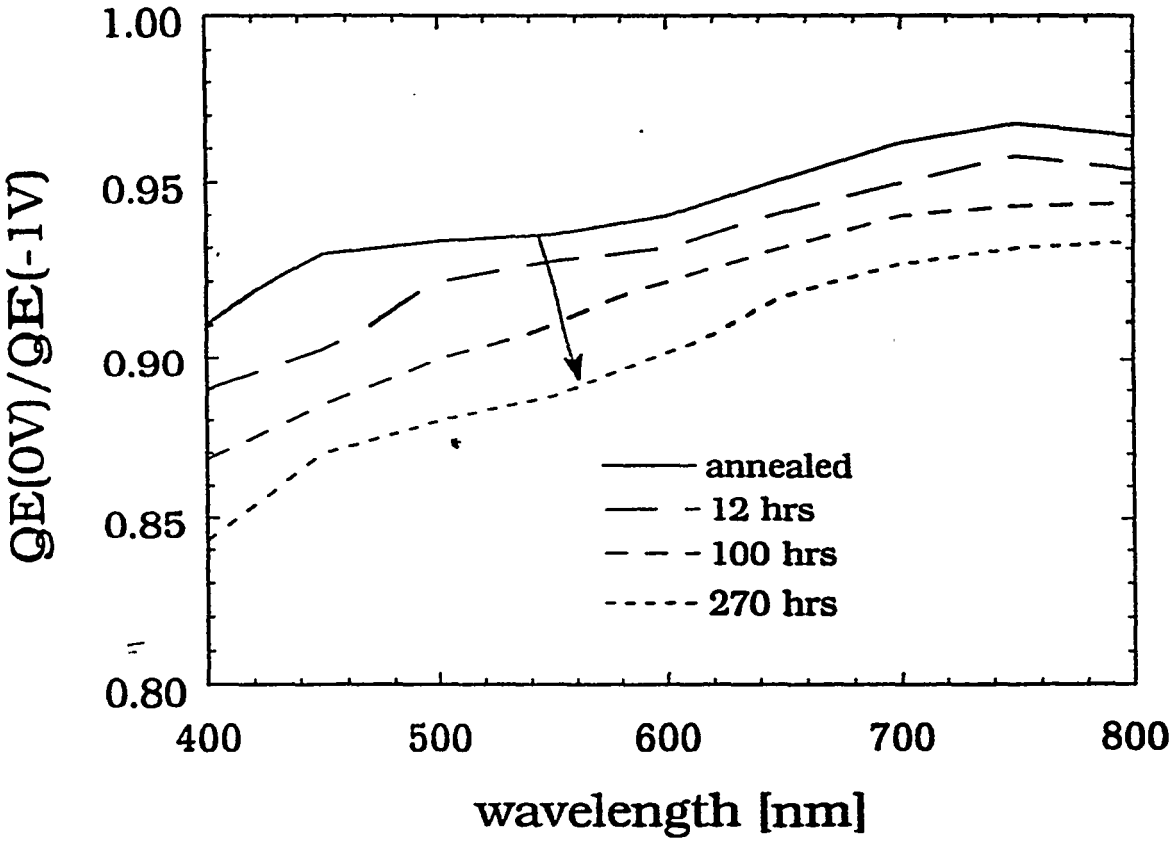

Figure 8. Effect of light soaking on voltage bias ratio of QE for front loaded a-SiGe device #3520.

Table 11. Initial and degraded (200 hours light soak) FF of front loaded and ungraded devices (1000Å) for illumination through p and n-layers. All a-SiGe E_G=1.4 eV.

Device	Illumination through	Condition	FF (%) AM1.5	red	blue
3548 front loaded	p	initial	48.3	52.3	51.0
		200 hours	45.0	47.7	45.8
	n	initial	52.2	51.0	55.3
		200 hours	48.4	48.2	50.0
3562 ungraded	p	initial	31.5	30.5	35.0
		200 hours	29.9	28.0	33.0
	n	initial	30.2	32.0	31.3
		200 hours	27.8	29.2	28.9

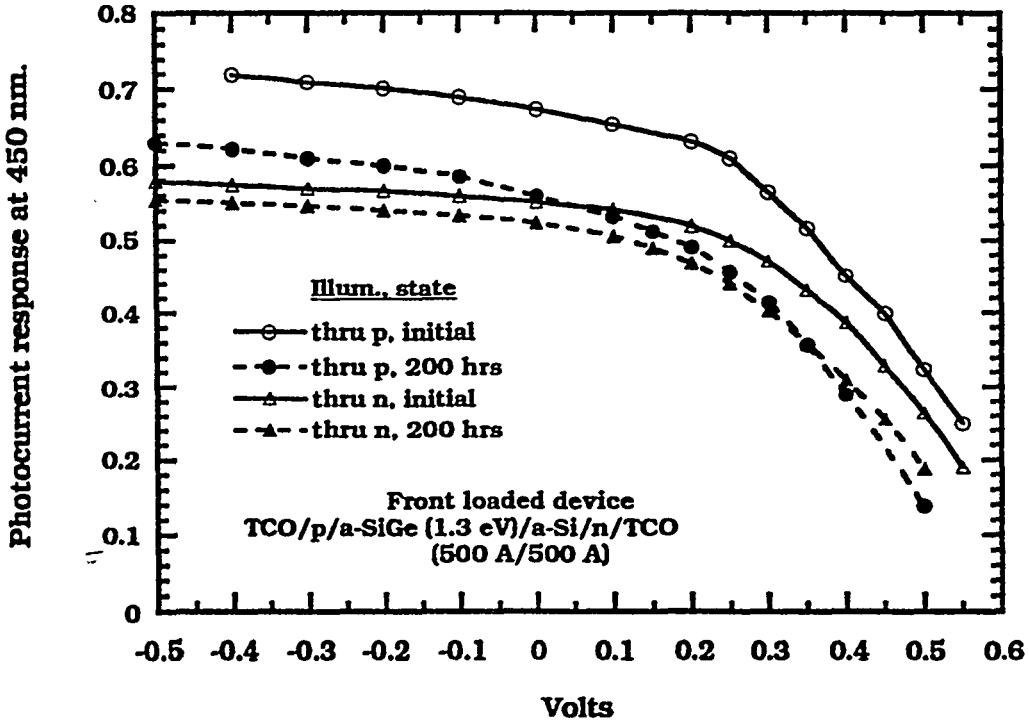

Figure 9. Voltage bias dependence of photocurrent at 450 nm for p,n illumination of front loaded a-SiGe device (#3548) in initial and light soaked state.

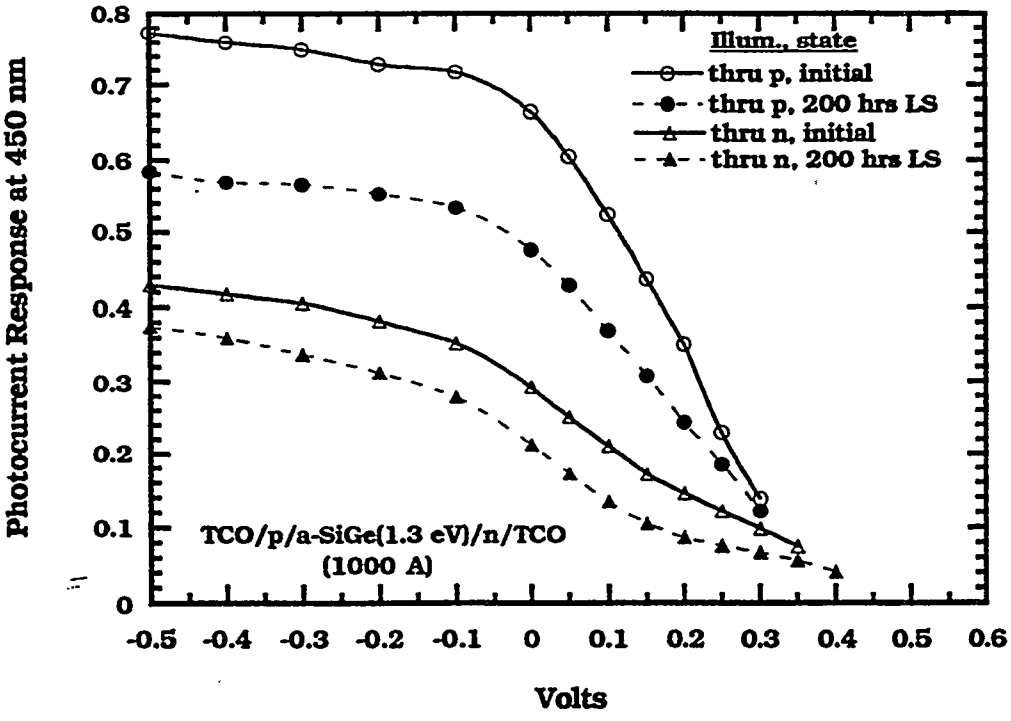

Figure 10. Voltage bias dependence of photocurrent at 450 nm for p,n illumination of ungraded a-SiGe device (#3562) in initial and light soaked state.

3.2.3 a-SiGe Solar Cell Stability

The 1.4 eV front loaded device from Table 10 and an ungraded 1.4 eV a-SiGe device (1000Å) were light soaked for 200 hours. Figures 9 and 10 show the photocurrent response for strongly absorbed 450 nm chopped light for p and n-illumination in the initial and degraded state for both devices. Comparing the initial curves, it is apparent that the front loaded device has much better hole collection than the ungraded device (QE=0.56 vs. 0.29 at 0 Volts) but they have comparable electron collection (QE~0.70 at OV). In both cases, the change with light soaking in electron collection (through p-layer) is **greater** than the change in hole collection (through n-layer). This is supported by the spectral dependence of the QE ratio in Figure 8. In fact, the electron and hole collection are nearly equal in the degraded state for the front loaded device (dashed lines of Figure 9).

The FF for full AM1.5, red and blue filtered light for p and n-illumination is given in Table 11 for these two devices. The ungraded a-SiGe device has higher FF for blue light through the p-layer compared to blue light through the n-layer. This is opposite the front loaded device, supporting the conclusion that front loaded grading improves the hole collection more than electron collection. The degraded FF of the front loaded device is always much higher than that of the ungraded device for all illumination conditions. We have found that 1000Å a-Si cells degrade about 5%. This suggests that a small but fixed amount of degradation may be due to the interfaces. The effect of a residual interface component of degradation needs to be evaluated.

3.2.4 Discussion of Electron and Hole Contribution to Stability in a-SiGe Solar Cells

We have presented a self-consistent set of results showing that the primary benefit of the front loaded design for a-SiGe devices is improved **hole** collection, in agreement with modelling and results of others (15,16). It is also evident that the electron collection degrades more than the hole collection with extended light soaking (200 hours). However, this latter conclusion, which is based on **device** results (FF and chopped photocurrent bias dependence) is inconsistent with stability studies on a-SiGe **films**. We and others have found that the photoconductivity of low bandgap a-SiGe is unaffected by light soaking (20-22) while the hole diffusion length may decrease by 50% with light soaking (23). Thus, film results suggest that the electron $\mu\tau$ is unaffected by light soaking while the hole $\mu\tau$ decreases slightly. This is in contradiction to our device results. Possible explanations are that light soaking generates defects which alter the field profile in the device in a manner which degrades electron collection more than hole collection, or interface-

related defect creation. This dilemma will be addressed in future work. Results of smoothly graded front loaded cells having better performance than the diagnostic devices discussed here will be studied.

3.3 DISCUSSION AND COMPARISON OF a-SiGe FILM AND DEVICE CHARACTERIZATION

For purposes of specific comparison of measurements, we compare films of similar composition and bandgap. We compare the optical absorption results on #3534 (Figure 6) to the capacitance results on #3481 (Table 8) since they both had approximately 45% Ge corresponding to a bandgap of 1.4 eV. We also compare the capacitance results from Table 8 of the film with higher Ge content, #3420, to our measurements reported over the past several years on films and devices of similar composition (60% Ge) and bandgap (1.3 eV).

The sub-bandgap absorption from DBPC of #3534 in Figure 6 gave an Urbach energy of 59 meV, which is much larger than the 45-50 meV found for a-Si, and a deep defect density which is 20-30 times larger than reported for a-Si, by similar techniques. There was negligible increase in the deep defect density with light soaking implying very stable material. In contrast, the transient photocurrent and capacitance analysis of #3481 from Table 8 gives a lower Urbach energy of 52 meV, which is only slightly larger than for a-Si, and a deep defect density increased by a factor of 3 with light soaking. Thus on three basic properties - Urbach energy, increase in deep defects with alloying, and increase in deep defects with light soaking - the absorption data from Penn State and capacitance data of University of Oregon are in disagreement. Note that the Urbach energy in both cases is determined from a photocurrent technique.

Our measurements of the Urbach energy using sub bandgap QE in p-i-n cells gives 45 meV for a-Si and 45-50 meV for up to 60% Ge (12,13). A nearly constant Urbach energy over this range of Ge is consistent with reports of others for device quality a-SiGe alloys, and with the data of Table 8 except for film #3420 where it increases. Based on the small or negligible increase in Urbach energy, Ge content is expected to have little effect on the hole mobility.

The product of the transient hole $\mu\tau$ with the defect density in Table 8 is scattered but shows no trend with increasing Ge. For example, the product of $\mu\tau_p N_D$ is 2.4E7 for the a-Si film and 1.4E7/cmV for 3481 with 47% Ge, suggesting that the hole drift mobility is not affected by alloying. This is in agreement with results of others (24,25). In contrast, steady state hole $\mu\tau$ products show a smaller dependence on Ge alloying, decreasing by a factor of 2-4, and little degradation with light soaking (23). We conclude that the transient hole transport properties are not

well correlated with steady state behavior since the dramatic decrease with alloying and with light soaking is not seen in SSPG measurements or bifacial device results.

We have characterized the midgap defects by steady state capacitance on p-i-n cells (26) and found that 1.3 eV a-SiGe has 20-30 times more midgap states than a-Si. Further, if one makes the usual assumption that the defect band is 0.3 eV wide, then results of defect density (in cm^{-3}) from Table 8 are in good agreement with our capacitance results for midgap density of states (in cm^{-3} eV^{-1}) for a-Si and 1.3 eV a-SiGe. We also have found that low bandgap a-SiGe was very stable, based on lack of any change in photoconductivity during 270 hours of light soaking (20).

Taken as a whole, these results suggest that the deep defect density near midgap in the initial state increases significantly with Ge alloying. Optical absorption and capacitance disagree over the amount of increase in defects with light soaking. The transient hole $\mu\tau$ is apparently unrelated to the steady state behavior since the dramatic decrease with alloying or with light soaking are not seen in SSPG results or device performance.

3.4 NUMERICAL MODELING OF ALLOY SOLAR CELLS

Analytical modeling of the effect of a mobility gradient on solar cell performance was compared to the Penn State AMPS model. It should be emphasized that the output of these numerical models is highly sensitive to the input parameters. For the input parameters chosen, both ours and the Penn State model show that a poor mobility material in the front of a graded band gap p-i-n solar cell would result in a high electron concentration in the back of the device (see Figure 11). In principle, this large electron concentration would result in enhanced recombination losses if the electron lifetime was equal to or less than its value in amorphous silicon.

3.5 MODELS FOR MULTI-JUNCTION SOLAR CELL OPTIMIZATION

The current-voltage behavior of several photo-CVD a-SiGe:H and a-Si:H solar cells with different grading schemes were measured. Single and multijunction devices from Solarex were also characterized. The data was analyzed to obtain lumped diode parameters with SPICE circuit model software. These parameters were used to model the performance of multi-junction solar cells.

Photo-CVD solar cells were measured, including standard a-Si:H (#3396) and two alloy (1.3 eV band gap) front loaded solar cells, one (#3380) with smooth grading and, the other (#3520) with abrupt grading. Descriptions of these grading schemes is detailed elsewhere (1,2). Testing included J-V measurements at 25°C with the voltage ranging from -0.2 to 1V. Illumination

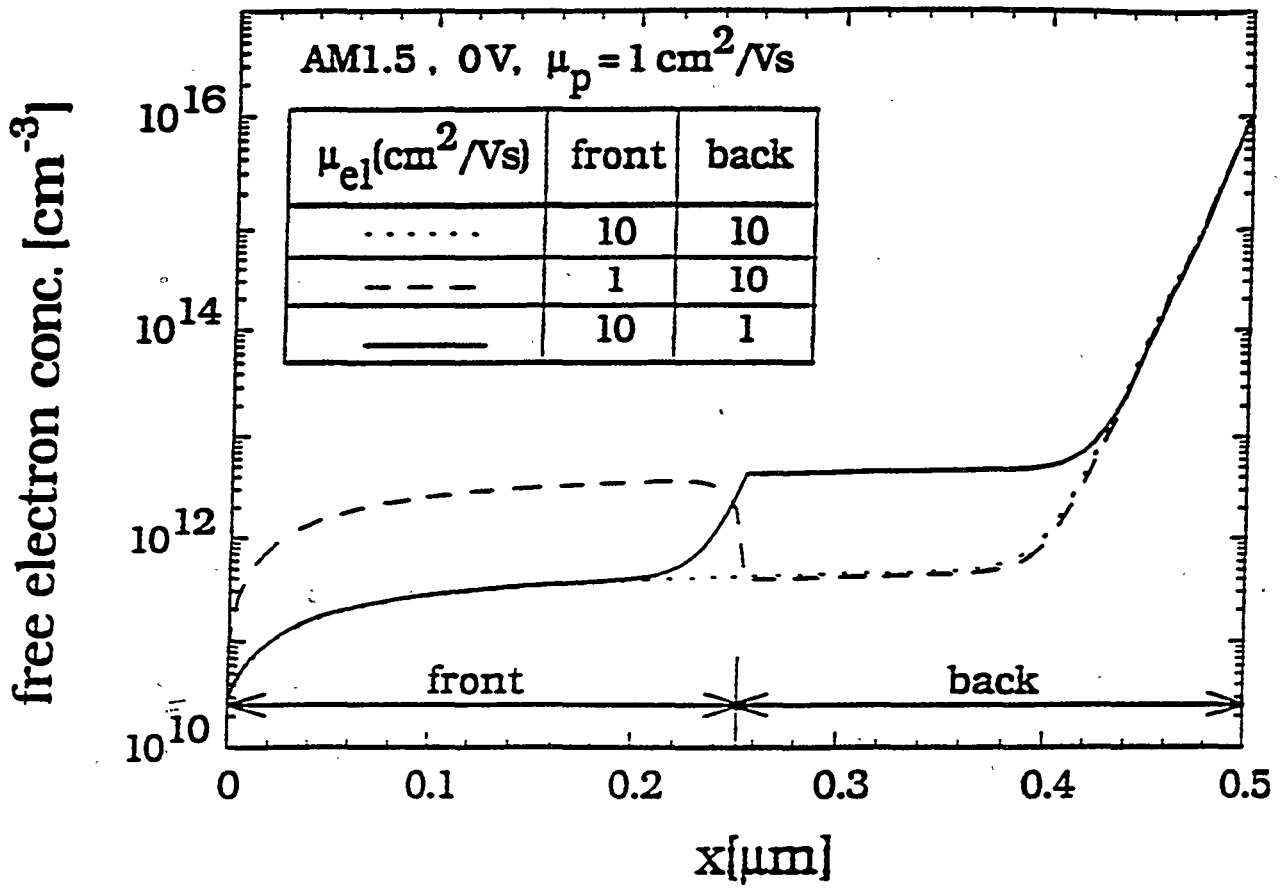

Figure 11. The effect of mobility gradient on the carrier density of a uniform bandgap p-i-n solar cell.

levels included dark, AM 1.5 @ ~ 100 mW/cm^2 with ELH lamp and red filtered ELH illumination (to approximate illumination levels found in the second p-i-n of a multi-junction solar cell).

The illuminated diode behavior was assumed to have a constant light generated current (J_L). With the addition of a shunt-like term (GV) to improve the fit, the following is obtained:

$$J_m(V)+J_L-GV=J_o\exp(BV) \qquad (2)$$

where $J_m(V)$ is the measured current and J_L was taken as either J_{sc} or $J(V=-0.2)$. The value of G was varied to obtain the best fit. The temperature dependence was not explicitly investigated, therefore B was equated to q/AkT for the temperatures studied since SPICE models require that a value of A be defined.

Typical results are given in Table 12 and Figures 12 and 13. We found that differences between solar cells on a given substrate were largely related to the values of G. The best fit value for G is strongly coupled to the choice of J_L. The values of A in the dark were 1.9 to 2.0 while under illumination values ranged from 3.0 to 5.0. The shunt term G was negligible in the dark on all devices indicating it was not a physical shunt. We interpret the value of G in the light as representing a voltage-dependent current collection mechanism. Figures 12 and 13 clearly show that G dominates the JV behavior at low forward bias. A, G and J_o were intensity dependent but not spectrally dependent. Therefore, values under solar spectrum or red light illumination were approximately the same.

J-V curves were generated by the SPICE software using A, J_o, R, G and J_L as inputs to a lumped circuit model consisting of a diode, resistor, shunt, and current source. Figure 14 compares the SPICE diode model to the measured values of #3396 and #3520. The SPICE values were calculated with parameters in Table 13. Note the close agreement between values extracted from measured

Table 12

Results of fitting illuminated measured J(V) data to equation 2. Devices were deposited by photo-CVD. #3396 was a standard a-Si p-i-n cell. #3380 and #3520 were front loaded while #3394 was ungraded a-SiGe.

Sample #	i-layer	Illum.	J_L (mA/cm^2)	G (mS/cm^2)	J_o (mA/cm^2)	A
3396	a-Si:H	a	9.0	1.6	3.5E-4	3.2
3380	a-SiGe:H	b	4.0	1.0	7.0E-3	4.4
3394	a-SiGe:H	b	4.0	0.5	1.6E-1	5.5
3520	a-SiGe:H	c	17.0	1.0	9.0E-2	4.4
		b	9.0	2.1	1.6E-2	3.6

Illumination conditions:
a) ELH at ~40 mW/cm^2 to obtain J_L comparable to tandem.
b) ELH with red filter (RG610) to simulate bottom cell.
c) Full ELH ~100 mW/cm^2

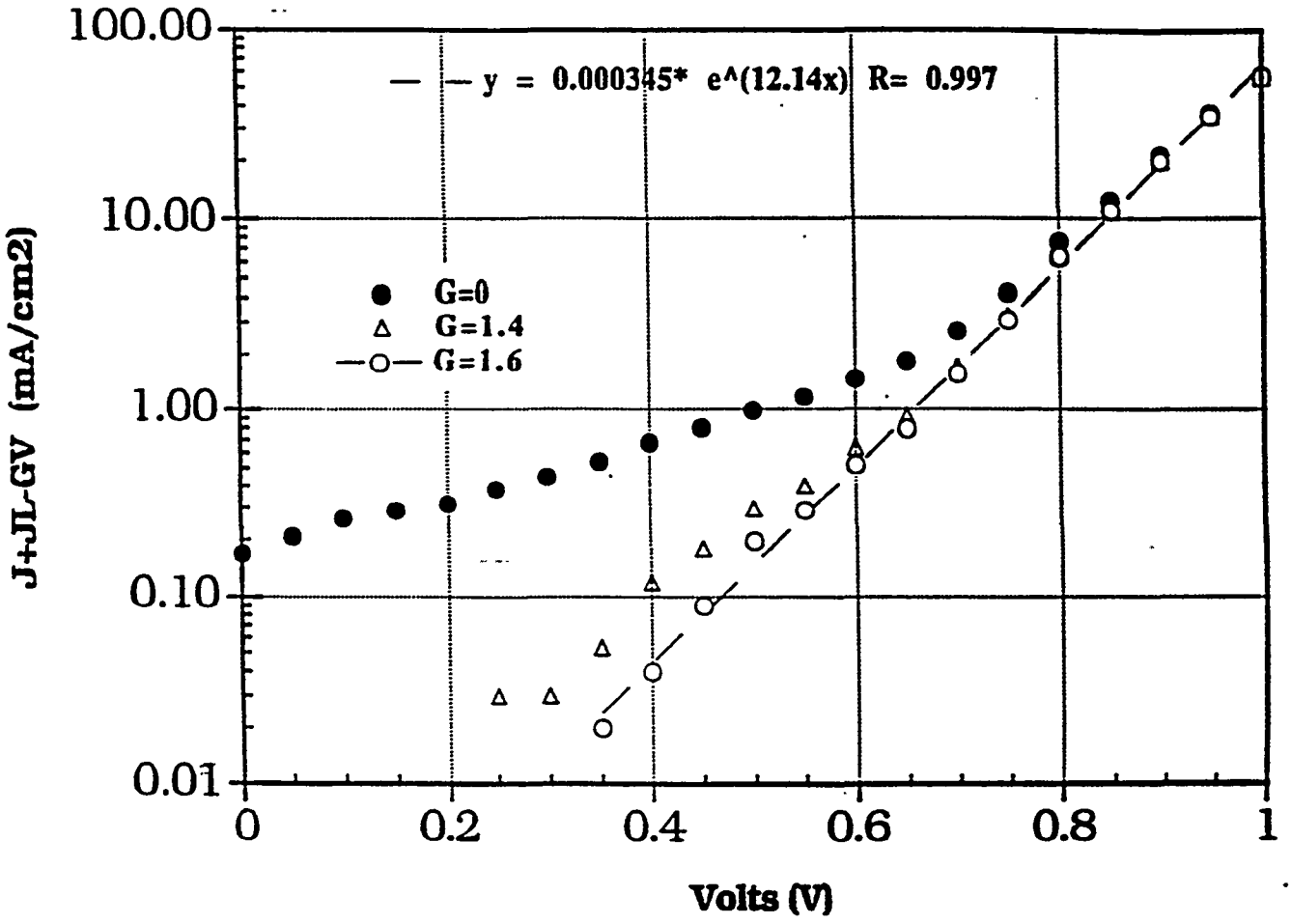

Figure 12. J(V) corrected for J_L and fixed shunt for an a-Si:H solar cell (#3396) under ELH illumination (J_{sc}=9 mA/cm^2).

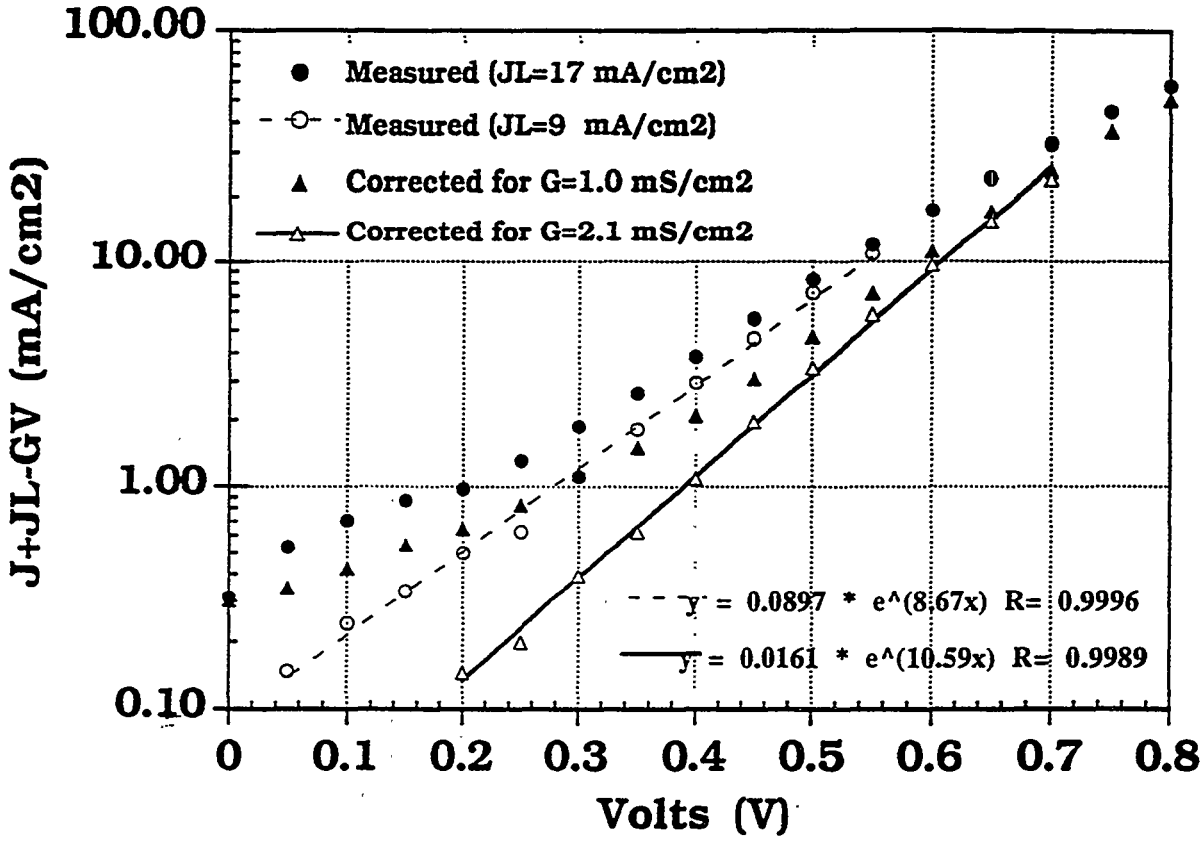

Figure 13. Measured and calculated (SPICE) data for an a-SiGe:H solar cell (#3520). Shown are the input parameters in mA/cm^2, S/cm^2, and ohm/cm^2 respectively.

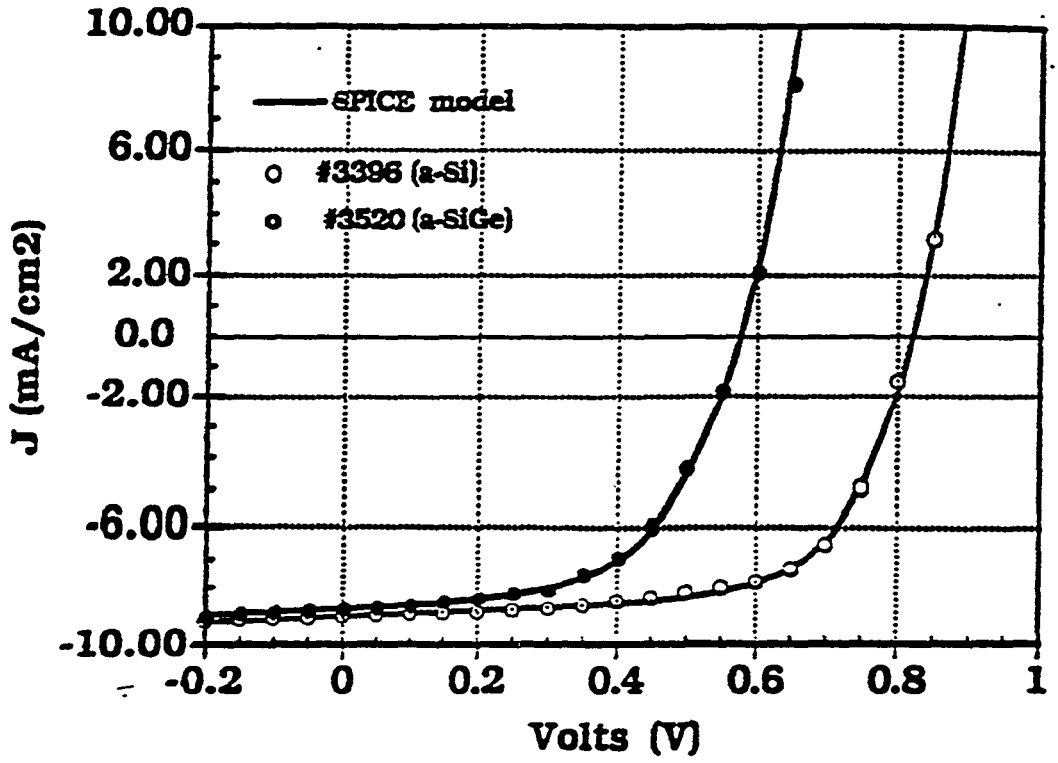

Figure 14. Measured and calculated (using SPICE) JV data for IEC devices #3396 (a-Si) and #3520 (a-SiGe). Calculated values determined with parameters of Table 13.

data in Table 12 and those giving the "best fit" to data using the SPICE program in Table 13.

Tandem solar cell modeling with the SPICE circuit analysis program proceeded using devices provided by Solarex Thin Film; a tandem a-Si/a-SiGe cell (L1318), and single junctions of a-Si (L1324) and a-SiGe (L1331). The single junction devices were representative of the two junctions which were used in the tandem. The JV behavior was measured under ELH (L1318 and L1324) or red (L1331) illumination adjusted to yield the same J_{sc} as obtained in the tandem under a simulator at 100 mW/cm^2, AM1.5. The illuminated JV characteristics of the two single junction cells were fit from 0 to 1 Volt using SPICE with fixed elements R, G, J_L and diode parameters J_o and A. Results are shown in Figure 15. Note the very close agreement over 3 orders of magnitude in current. The SPICE data was calculated using parameters given in Table 13.

Table 13

Results of fitting illuminated J(V) data to diode circuit model. Samples 3396, 3520 are from IEC, L1324 and L1331 are from Solarex.

Sample #	i-layer	J_L (mA/cm^2)	G (mS/cm^2)	J_o (mA/cm^2)	A	R (Ω-cm^2)
3396	a-Si:H	9.0	1.6	3.5E-4	3.2	0.1
3520	graded a-SiGe:H	9.0	1.0	2.2E-2	3.7	0.5
L1324	a-Si:H	8.6	0.8	2.1E-3	3.8	1.0
L1331	graded a-SiGe:H	8.6	0.8	1.4E-2	4.1	0.9

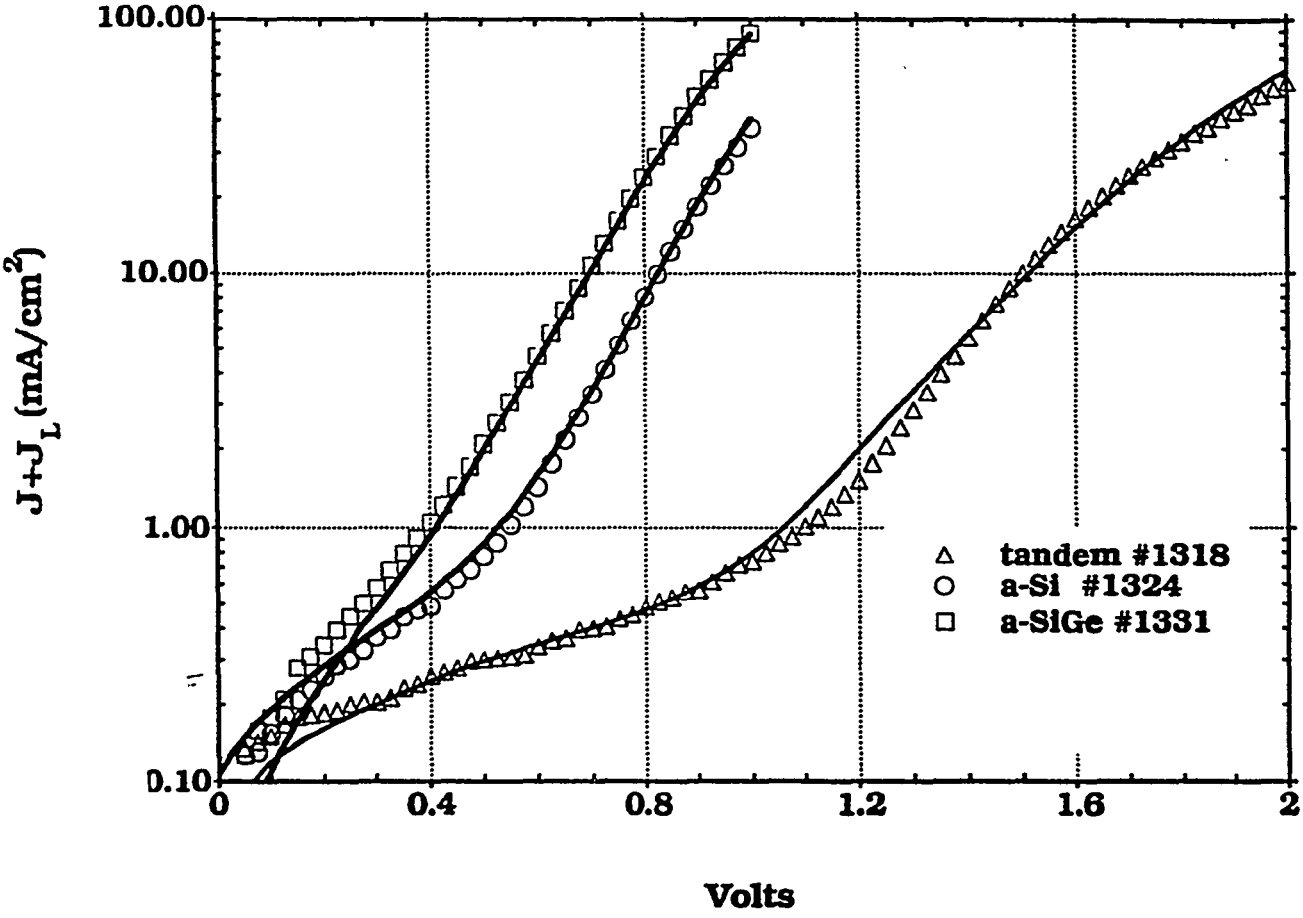

Figure 15. Measured (symbols) and calculated (lines) JV data for Solarex single and tandem cells. SPICE calculations of #1324 and #1331 were made with parameters of Table 13, #1318 with parameters of Table 15.

A SPICE model of a tandem cell was constructed using the single junction parameters of Table 13, without any additional resistance or diode as might be expected to reduce performance due to the n/p interconnect junction. Surprisingly, the SPICE tandem cell analysis using these single junction parameters yielded poorer performance than was actually measured on the tandem device. In order to obtain a better match to the measured data, G, J_o and A had to be reduced (to improve FF) on both sets of cell parameters. The resistance had to be increased to match the JV curve beyond V_{oc}. We used the results of fitting the two single junction devices (Table 13) as criteria in fitting the tandem cell as follows: J_o values should differ by 5-10 between the a-Si and a-SiGe devices, the device with the lower J_o should have a lower A factor by 10-20%, and the R and G values should be very similar. Table 14 gives the measured and predicted performance (using the "best fit" from single junction parameters and "better fit" to the tandem JV curve itself) while Table 15 gives the SPICE parameters used for each of junction models in the tandem model.

The J_o values of the single junction components in Table 15 are each almost an order of magnitude lower than the single junction of Table 13. An even better fit to the measured data is possible by reducing J_o and A of each cell even more. Clearly it was not necessary to introduce loss mechanisms to the tandem cell model (such as a tunnel junction) in order to fit the measured data on this Solarex device. On the contrary, the results suggest that each device has better performance when in the tandem configuration. Future work will involve investigating the effect of tunnel junctions and current mismatch on tandem cell performance using parameters as in Table 15. This is important since it is likely that tandem devices fabricated initially at IEC will not have optimized tunnel junctions as found in the Solarex cells. The modeling will help us to recognize the influence of tunnel junctions on overall performance of IEC tandem devices.

Table 14

Measured and calculated tandem cell performance

	V_{oc}	J_{sc}	FF	Max. Power (mW/cm^2)
L1318 (measured)	1.512	8.6	66.5	8.64
SPICE (using single junction best fit parameters of Table 9)	1.490	8.6	59.5	7.54
SPICE (using better fit tandem parameters of Table 11)	1.510	8.6	65.0	8.34

Table 15

SPICE parameters of each junction used to model tandem cell L1318. Performance given in Table 14.

	R (Ω)	G (mS)	J_L (mA/cm^2)	J_o (mA/cm^2)	A
Junction 1	1.5	.4	8.6	$3x10^{-4}$	3.1
Junction 2	1.5	.4	8.6	$3x10^{-3}$	3.4

SECTION 4.0

HYDROGEN EXPLOSION AND HAZARDOUS GAS SAFETY

An explosion occurred in the amorphous silicon deposition laboratory at the Institute of Energy Conversion on September 1, 1992 when a large quantity of high pressure hydrogen gas was accidentally routed to a line intended for vacuum purging. A flexible stainless steel hose segment ruptured, releasing high pressure hydrogen gas into a reactor enclosure. The plexiglass walls of the enclosure blew outward causing extensive damage to the laboratory. There was no evidence of heat, smoke, or fire. No one was in the room at the time and no one was injured. A Department of Energy accident investigation team conducted a formal investigation of this incident and its underlying causes.

This report will examine the sequence of events that led to the hydrogen explosion and the specific causes. The findings of the subsequent investigation and modifications to the gas handling system, facility, and procedures that have been made partly as a result of those findings will be detailed. Finally, some of the lessons learned and strategies for preventing this type of accident in an academic research laboratory using these hazardous gases will be discussed.

Background

The a-Si laboratory at IEC contains two reactors for the investigation of a-Si materials and devices, a photo-assisted CVD reactor and a plasma-assisted CVD reactor. The reactors are located in separate ventilated enclosures. The deposition of a-Si in these reactors utilizes hydride gases including silane, germane, diborane, phosphine, and methylsilane as well as hydrogen. These gases are stored in ventilated, sprinklered explosion proof gas cabinets in an adjacent room. The gases flow through seamless gas lines from the cabinets to the reactor enclosures as shown in Figure 16. In addition, hydrogen selenide, which is used for selenization experiments is stored in the gas cabinets.

A number of measures to ensure safety in the handling of these gases were in place prior to this incident. Safety at IEC has been an active priority supported at the top administrative level and an active safety committee has been in place for 16 years. Specific safety measures for the use of the hazardous gases included:

* Hazardous gases are stored in ventilated and sprinklered gas cabinets.

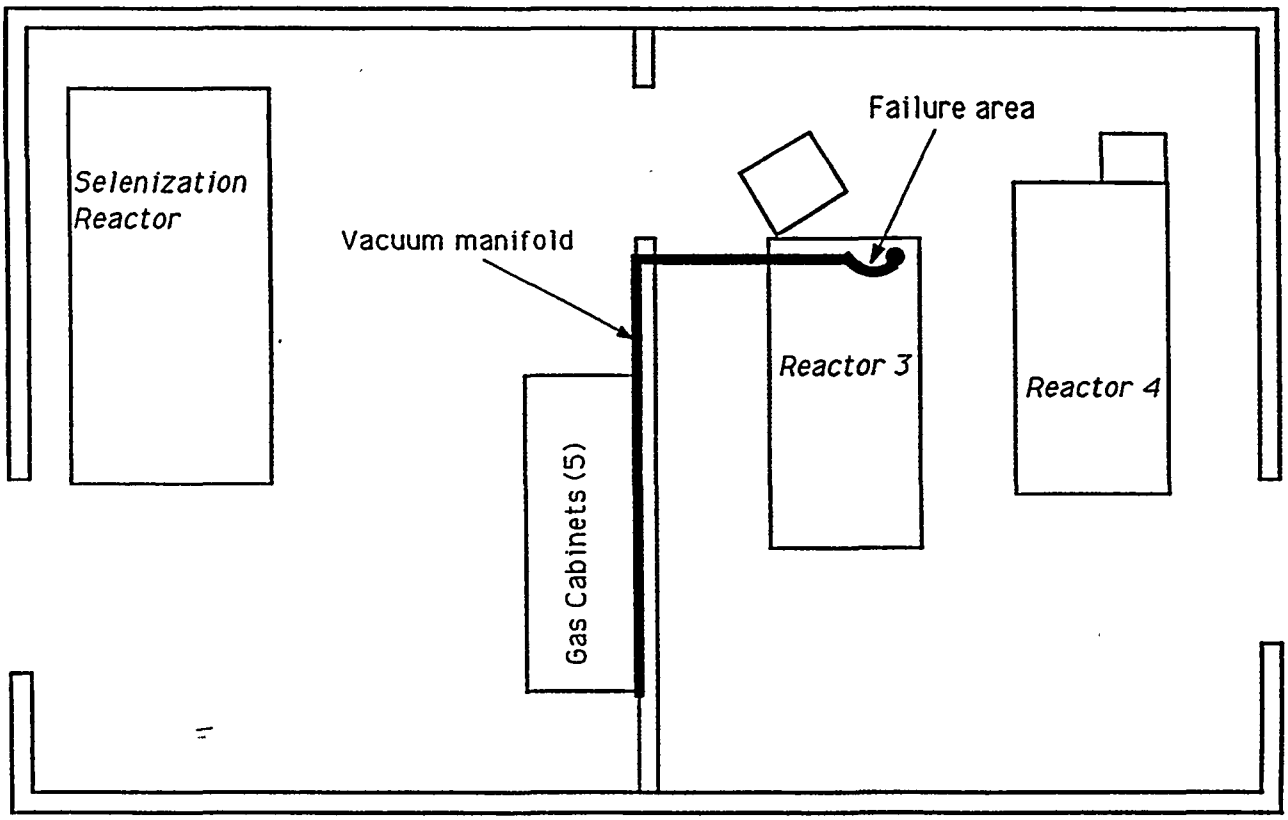

scale: none

Figure 16. Layout of laboratories where hazardous gases are stored and used.

* A multipoint hydride gas detection system manufactured by MDA continuously monitors for the presence of hydride gases in the experimental enclosures, gas cabinets, or room ambients.

* Interlock circuits ensure that all hazardous gas flows shut off automatically in the event of a loss of ventilation, gas detection, power loss, or other alarm in the building.

* Ventilation for the experimental enclosures and gas cabinets is regularly measured and continuously monitored to determine if there is a failure.

* A diesel generator is in place to provide backup power in the event of a power failure. This ensures that ventilation, gas monitors, alarm, and emergency shutoff features remain on line.

* The pressure in the reactor lines is continuously monitored during experiments and automatically shuts off gas flows in the gas cabinets in the event of an unexpected increase or decrease.

* The gas handling systems were state-of-the-art at the time of installation and included excess flow shut-off valves, air-actuated high pressure safety valves, and high purity single stage, stainless steel regulators.

* Pyrolysis stacks on the reactor exhausts ensure that unreacted gases are not released into the atmosphere.

Prior to this incident there have been no significant safety problems related to the amorphous silicon deposition laboratory.

Accident Sequence

The sequence of events that lead to the incident is given below. Figure 16 shows the layout of the rooms, where the hydrogen gas cylinder is stored in an explosion proof gas cabinet, and the adjacent room where the explosion occurred in the photo-CVD reactor enclosure. Figure 17 shows a schematic of the hydrogen gas handling system within the gas cabinet and to the reactor at the time of the incident. A schematic of the photo-CVD reactor is shown in Figure 18.

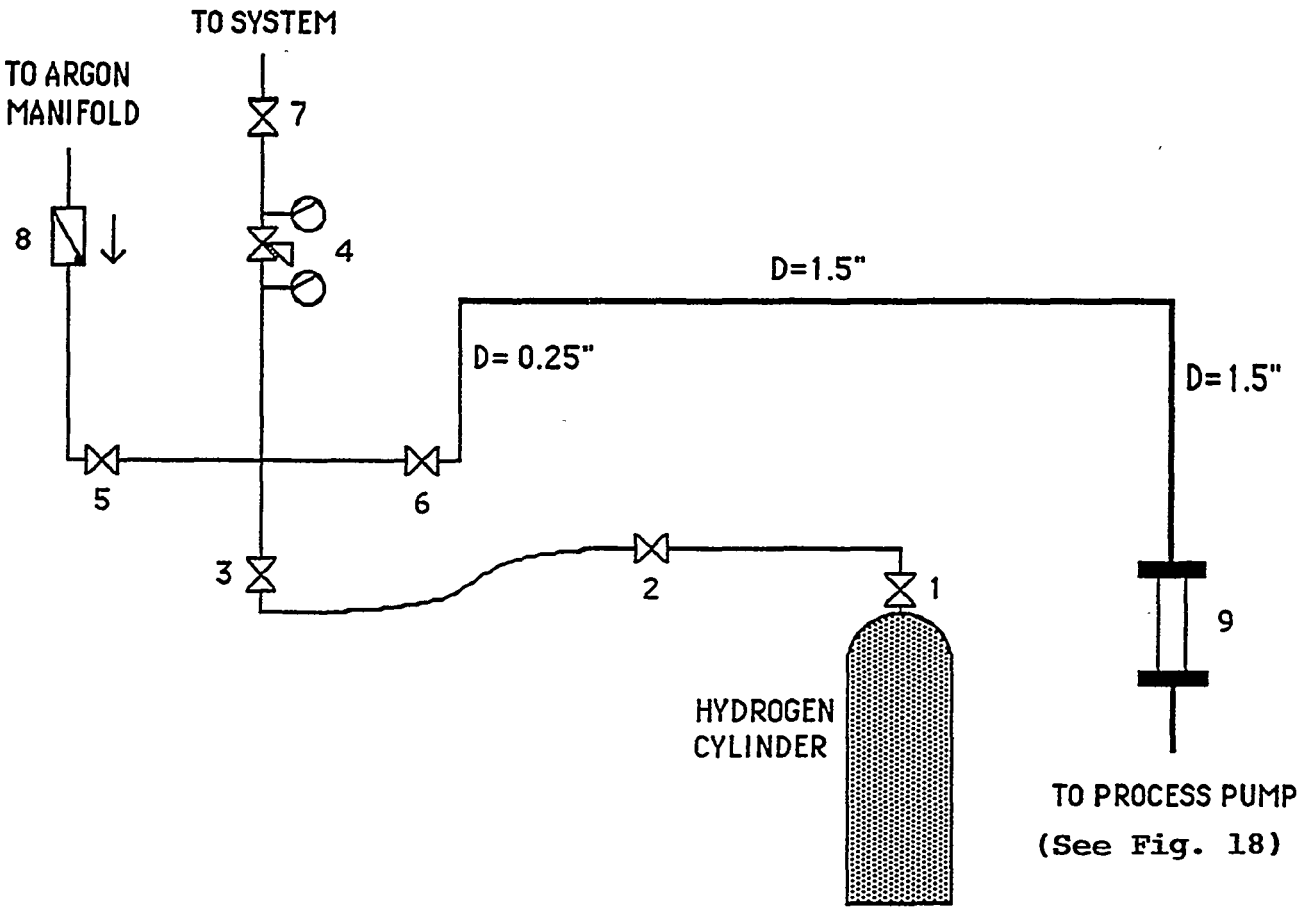

1 HYDROGEN CYLINDER VALVE
2 EXCESS FLOW VALVE
3 HIGH PRESSURE SAFETY VALVE
4 REGULATOR
5 PURGE VALVE
6 VACUUM VALVE
7 ISOLATION VALVE
8 CHECK VALVE
9 BELLOWS ADAPTER

Figure 17 Hydrogen gas handling system prior to explosion.

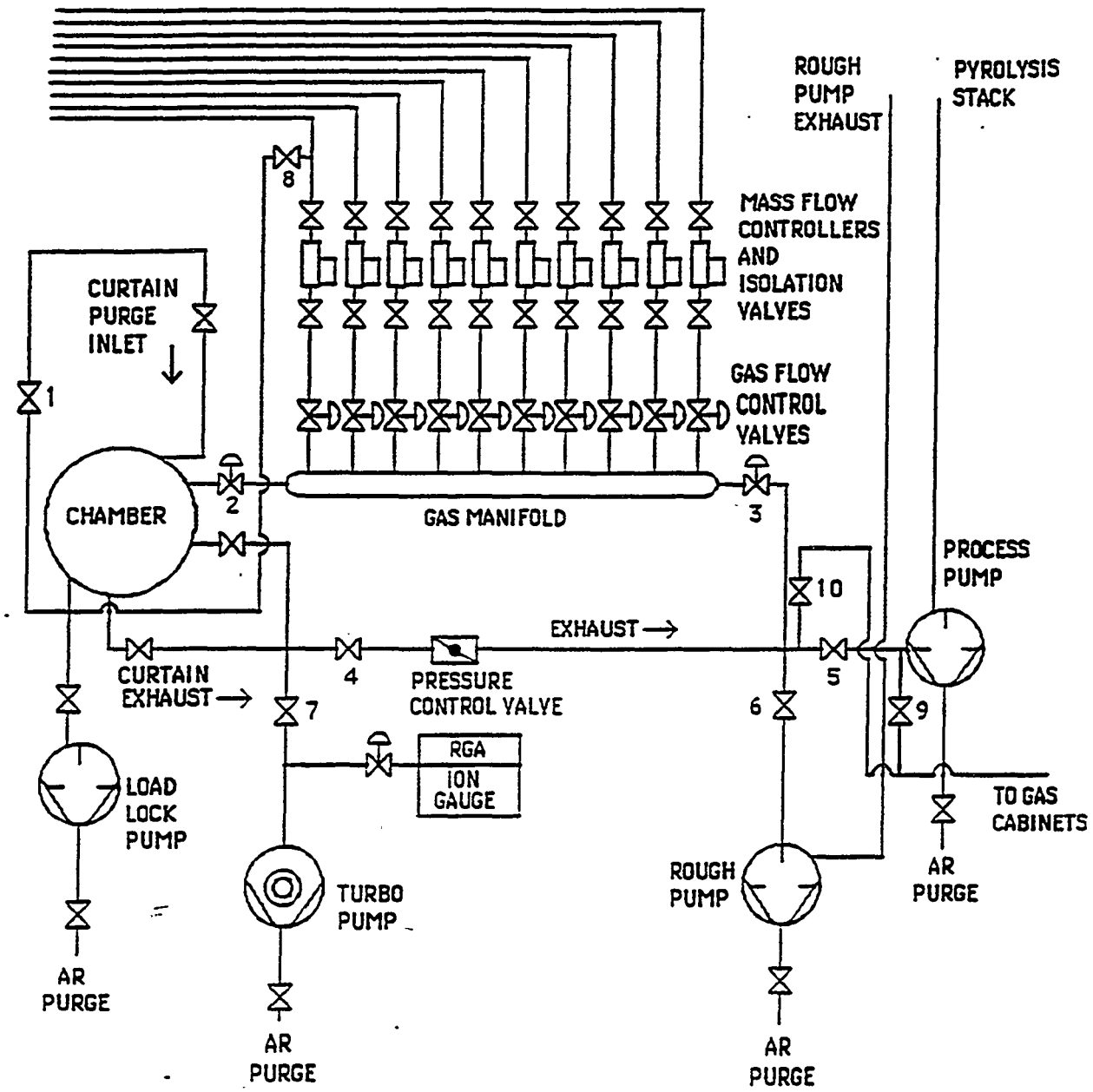

Figure 18 Photo-CVD reactor layout.

August 27, 1992

1. During a standard deposition in the photo-CVD reactor, the H_2 flow rate dropped from the setpoint, 50 sccm, to <25 sccm.
2. The cylinder pressure reading on the regulator was 0 psig on the high pressure gauge and 5 psig on the low pressure gauge.
3. The excess flow valve was reset 3 times with no change in gauge pressure.
4. The high pressure safety valve was confirmed to be open.
5. It was concluded that the H_2 cylinder was empty and a new one was ordered.

September 1, 1992

1. The new H_2 cylinder was received and preparations to change the cylinder were made.
2. The pump valve was opened to allow the gas manifold to be evacuated.
3. The vacuum pump exhaust purge flow was set to 1000 sccm.
4. The hydrogen cylinder valve was closed. It was tight and difficult to turn.
5. The high pressure safety valve was opened from the switch on the safety panel.
6. The excess flow valve was opened manually to purge position.
7. No change was seen in the pressure readings on the regulator.
8. The vacuum valve in the gas cabinet was opened.
9. The low pressure gauge on the regulator dropped to vacuum range, -30 in. Hg.
10. The thermocouple gauge at the process pump read ~ 5 μm Hg.
11. Within 1 minute, with no one in the lab, a loud, dull "pop" was heard by several people in nearby labs.
12. All equipment in both labs was checked with no indication of anything wrong. The system was left to pump for about 1 1/2 hours with no further incidents.
13. The pump valve was closed and it was decided to shut down the system for further evaluation.
14. The cylinder valve was opened slightly so that it could be re-seated to ensure that it was completely closed. At this point the excess flow valve and vacuum valve were still open.
15. A sound of rushing gas flow was heard and the pressure at the regulator rose to at least 1100 psig.
16. The cylinder valve was turned to close but was still very tight and hard to turn.
17. The explosion occurred in the a-Si deposition lab at 11:45 a.m. It was heard throughout the building.
18. The building alarm sounded 5-10 seconds after the blast. The alarm automatically shut off the high pressure safety valve.

The University of Delaware Department of Occupational Health and Safety along with the local fire department responded to the incident. Representatives entered the building in Self Contained Breathing Apparatus (SCBA) and monitored for gases with hand-held hydride and combustible gas detectors. There was no detection of hazardous gas nor any indication of smoke or heat in the gas cabinet lab. All gas cylinders in the gas cabinets were manually closed. The a-Si deposition lab was observed from the doorway. There was substantial damage to the room and the reactor enclosure, but no signs of heat, smoke or fire. The lab was checked with the gas detectors and no hazardous levels were found.

Both rooms were re-checked with a second combustible gas detector and then were sealed off to prevent entry before an investigation could be made. After an investigation by the city fire marshall, all equipment in the deposition lab was safely shut down, and all electrical circuits to the photo-CVD reactor were de-energized.

Accident Investigation and Follow-up

A preliminary investigation of this incident was conducted by personnel from IEC and the University of Delaware's Department of Occupation Health and Safety. This enabled identification of direct and contributing causes for the hydrogen release and a number of recommended modifications to the gas handling system to prevent similar releases in the future.

A formal investigation of the explosion and its contributing factors was conducted by a Department of Energy accident investigation team at the request of IEC. The team included Paul Moskowitz and Herb Schulman of Brookhaven National Laboratory, Caroline Scott of Fluid Control Systems, and William Griffing of NREL. Their investigation was conducted on September 22 and 23 following Department of Energy accident investigation protocols. Conclusions were made based on physical examination of the site and selected components of the gas handling system, review of the preliminary incident report, photographs, procedures, etc. and extensive interviews with IEC personnel.

The report that resulted from this accident investigation identified the direct cause, contributing factors, and root cause of the hydrogen explosion. The direct cause was found to the opening of a valve in the wrong sequence resulting in the release of hydrogen at pressure >1100 psi into a section of the vacuum system not intended to withstand high pressures. The resulting overpressure caused a bellows to burst releasing the hydrogen into the reactor enclosure. It was not determined whether the explosion was simply pressure-induced or if there was an ignition.

Several contributing factors were identified. This included the presence of at least one poorly operating component in the gas handling system, probably the excess flow valve, which had given a false indication that the hydrogen cylinder was empty. The report also found an outdated design for the system in general. In addition, a lack of formal written policies and procedures for cylinder changing, system operation, maintenance, and operator training was cited.

Finally, the root cause, which is the basic underlying reason for an incident to occur, was "related to the absence of a formal policy for the systematic oversight of gas handling and safety systems."

The accident investigation team also provided a list of suggestions to prevent a similar event from occurring in the future and to improve the safety of the hazardous gas operations in general. This list, along with the findings of the internal review, formed the basis of the subsequent upgrade of the laboratory and procedures.

To oversee implementation of the necessary modifications a Hazardous Gas Task Force was appointed and consisted of R. Birkmire, W. Buchanan, and W. Shafarman of IEC and J. Miller of the University of Delaware's Dept. of Occupational Health and Safety. The goal of this task force was to oversee restoration and upgrade of the amorphous silicon laboratory and to ensure that hazardous gas operations at IEC are designed and operated safely in the future.

To assist this process, the task force spoke with many of the laboratories and companies in the U.S. which use similar hazardous gases for solar cell research and development. This was very valuable, especially in determining how to best redesign and construct the gas handling system. It was found that there is considerable variation between different laboratories in the systems used for delivering hazardous gases to experiments and reactors.

Modifications to a-Si Labs.

A number of modifications were made to the amorphous silicon gas handling system, facilities, and procedures in response to the recommendations of the Hazardous Gas Task Force. Whenever applicable, the upgrade was also extended to the hydrogen selenide reactor. Many of the modifications were suggested by the report of the accident team. In addition, the "Safety Analysis Report For the Use of Hazardous Production Materials in Photovoltaic Applications at the National Renewable Energy Laboratory" was valuable in determining many of the upgrades.

The significant modifications are listed below. Figure 19 shows a schematic of the new gas handling apparatus. All hazardous gases have identical components and configuration.

A. Gas handling modifications.

1. An additional gas cabinet was added to room 142 so that each hazard class of gas could be stored in different cabinets and have dedicated purge cylinders. This required increased ventilation.

2. Gas cabinet vacuum lines were moved from the high pressure side of the regulator to the low pressure side.

3. Isolation valves were installed on the high pressure side of the regulator.

4. New excess flow valves from a different manufacturer were installed. The ones chosen were deemed more reliable than the previous model.

5. New tied-seat regulators were installed. A second regulator in line was considered in order to protect low pressure fittings downstream in the event of a regulator failure. An alternative was to limit cylinder pressures such that the excess flow valve closing would protect the low pressure lines. This was the option chosen.

6. All valves in the gas cabinets were either replaced with new valves, or rebuilt.

7. New gas cylinders with flow restricting orifices were installed.

8. Cylinder sizes and pressures were reduced to the smallest practical size. All cylinders are now required to contain less than 1000psi to ensure that the low pressure line and all components are able to withstand the pressure in the case of a catastrophic regulator failure, assuming that the excess flow valve functions properly.

9. Gas lines between the reactors were replaced, and all the gas lines between the gas cabinets and reactors were mechanically attached to supports.

B. Facility modifications.

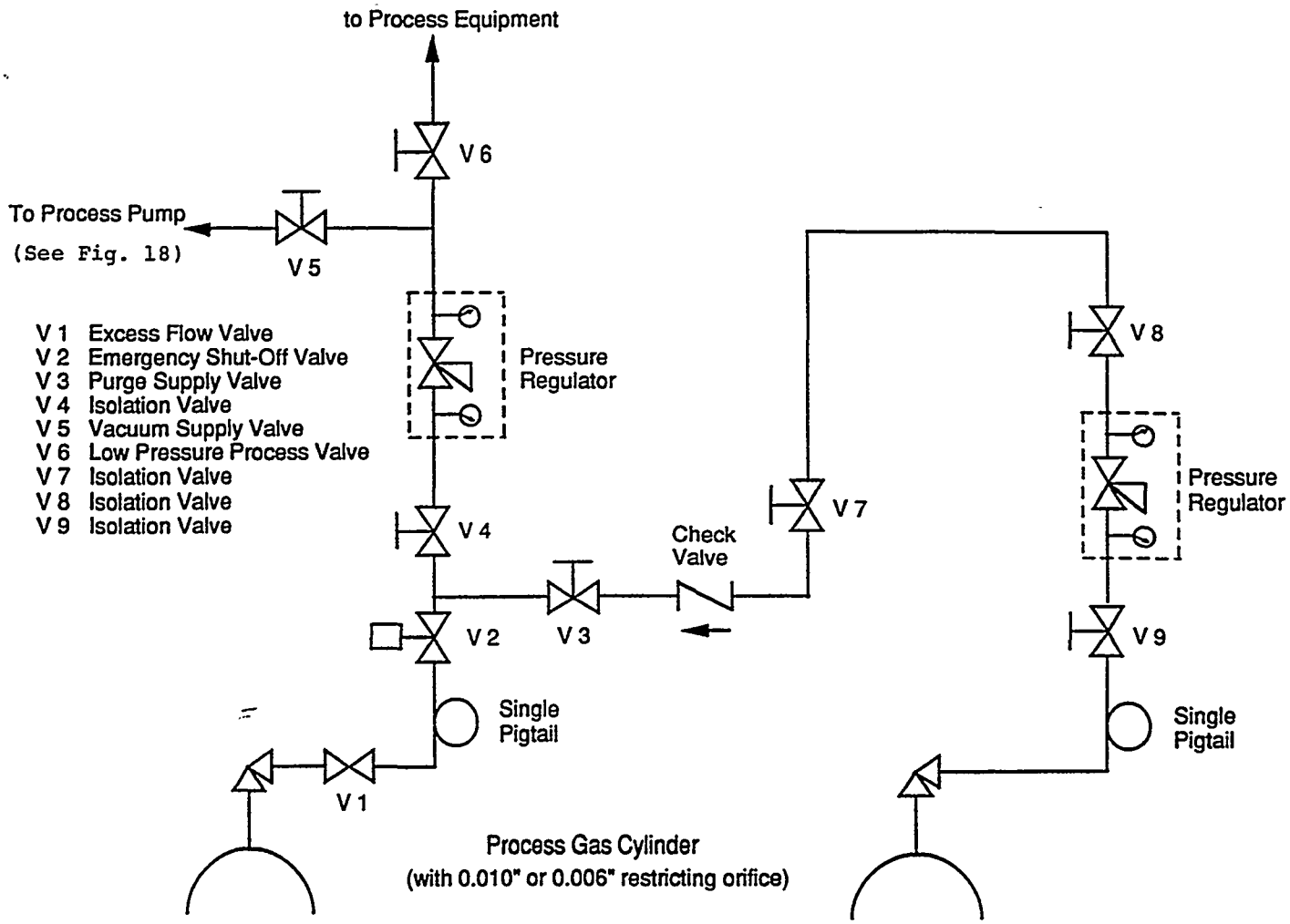

Figure 19 New gas handling system for all hazardous gases.

1. All laboratory entranceways were provided with swing-out doors and a viewing window.

2. A sprinkler system was added to the labs and entranceways.

3. On-line monitoring for hydrogen gas was implemented and interfaced to the building fire alarm system and automatic gas flow shut off interlocks.

4. Emergency shut-down buttons for the reactors were provided outside the lab doors.

5. Visual indicators were provided for hazardous gas alarms inside and outside the labs. Alarm buzzers were also added inside the labs.

6. The plexiglas reactor enclosures were replaced with polycarbonate.

7. A more informative enunciator panel was added to the building entrance to allow all gas alarms, sprinklers, etc. to be clearly indicated.

8. Placarding of all doors leading into lab areas, gas cabinets, gas lines, shut-off switches, etc. was provided.

C. Procedural Modifications

1. Formal safe operating procedures were completed including procedures for cylinder changing, system start-up and shut-down, maintenance, emergency procedures, etc. These were approved by the IEC Chemical Hygiene Committee.

2. Maintenance logs are posted in the labs to verify that all maintenance, as required in the safe operating procedures, is kept up-to-date.

3. Procurement of hazardous gas cylinders will require approval of the IEC Chemical Hygiene Officer to ensure that minimum quantities with flow restricting orifices are ordered.

All of the above modifications to the laboratories were completed before the amorphous silicon deposition systems were allowed to become operational. Due to the dedication of the IEC staff, these modifications were completed in under four months.

Conclusions

The direct cause of the hydrogen explosion is essentially clear, even though some of the details could not be positively determined. Consequently, actions needed to prevent similar incidents from recurring could be taken. This primarily involved redesign and construction of the gas handling system and establishment of more formal procedures.

Perhaps more important is the establishment of policies to ensure that the use of hazardous gases remains safe. This requires keeping up with all necessary maintenance and replacing or rebuilding components as needed. In addition, it is critical to provide routine re-evaluation of the equipment and procedures to keep up-to-date with the latest technological advances. Even though the amorphous silicon gas handling systems were state-of-the-art at the time of its construction, in less than 5 years some of the equipment and procedures had become outdated.

In a University laboratory with limited resources keeping up-to-date with safety advances is difficult. Making changes that may be recommended after routine re-evaluation will not always be possible without funding specifically targeted toward safety and independent of basic research funding.

SECTION 5.0

REFERENCES

1. IEC Final Report to SERI under subcontract XL-8-18092-1, 5/88 to 2/91 (1992).
2. C. Fortmann, S. Hegedus, T. Zhou, B. Baron, Solar Cells **30**, 255 (1991).
3. A. Asano, Appl. Phys. Lett. **56**, 53 (1990).
4. C. Fortmann et al., J. Appl. Phys. **64**, 4219 (1988).
5. E. Bhattacharya, A. Mahan, R. Crandall, J. Pankove, Appl. Phys. Lett. **54**, 1247 (1989).
6. W. Nevin, H. Yamagishi, M. Yamaguchi, Y. Tawada, Appl. Phys. Lett. **58**, 2669 (1991).
7. R. Crandall, A. Mahan, B. Nelson, M. Vanacek, I. Balberg, Proc. 6th PVSEC, New Delhi, 879 (1992).
8. C. Fortmann, R. Dawson, C. Wronski, Mat. Res. Soc. Symp. Proc. **219**, 63 (1991).
9. C. Fortmann, J. Cohen, Mat. Res. Soc. Symp. Proc. **258**, 383 (1992).
10. R. Street, Appl. Phys. Lett. **59**, 1084 (1991).
11. R. Dawson, et al., Mat. Res. Soc. Symp. Proc. **258**, 595 (1992).
12. IEC Annual Report to SERI, under subcontract XL-8-18092-1, 5/88 to 4/89 (1990).
13. S. Hegedus, et al., Proc. 20th IEEE Photovoltaic Spec. Conf., 129 (1988).
14. T. Unold, J. Cohen, C. Fortmann, Mat. Res. Soc. Symp. Proc. **258**, 499 (1992).
15. S. Guha et al., Appl. Phys. Lett. 54, 2330 (1989).
16. Y. Nakata et al., Mat. Res. Soc. Proc. Symp. **192, 15** (1990).
17. C.M. Fortmann, Proc. 21st IEEE PV Spec. Conf., 1493 (1991).
18. Misiakos et al., J. Appl. Phys. **64**, 383 (1988).
19. R. Arya et al., Proc. 20th IEEE PV Spec. Conf., 85 (1988).
20. IEC Final Report to SERI, under Subcontract XB-4-04061-1, 5/84-4/88 (1988).
21. G. Bauer, C. Abel, G. Schumm, 6th PVSEC, 339 (1992).
22. S. Aljishi, Z. Smith, S. Wagner, Advances in Amorphous Semiconductors (Fritzche, editor), World Scientific Pub. Co. 887 (1988).
23. Solarex Annual Report to SERI, under Subcontract ZB-7-060-03-2, 2/88-2/89 (1989).
24. R. Street, C. Tsai, M. Stutzmann, J. Kakalios, Phil. Mag. B **56**, 289 (1987).
25. F. Karg, W. Kruhler, M. Moller, K. Klitzing, J. Appl. Phys. **60**, 2016 (1986).
26. S. Hegedus, E. Fagen, J. Appl. Phys. **71**, 5941 (1992).

ABSTRACT

Results and conclusions obtained during a research program of the investigation of amorphous silicon and amorphous silicon based alloy materials and solar cells fabricated by photo-chemical vapor and glow discharge depositions are reported. Investigation of the effects of the hydrogen content in a-Si:H i-layers in amorphous silicon solar cells show that cells with lowered hydrogen content i-layers are more stable. A classical thermodynamic formulation of the Staebler-Wronski effect has been developed for standard solar cell operating temperatures and illuminations. Amorphous silicon germanium films were deposited by photo-CVD for specialized characterization at outside laboratories. Bifacial current voltage and quantum efficiency measurements on a-SiGe p-i-n solar cells were used to determine the effect of i-layer bandgap and lightsoaking on hole and electron collection. Methods have been developed to extract a lumped equivalent circuit from the current voltage characteristic of a single junction solar cell in order to predict its behavior in a multijunction device. The specific causes and sequence of events that led to a hydrogen explosion in the amorphous silicon laboratory are examined. Modifications to the gas handling system, facility, and procedures were made based on a formal investigation of the incident. Finally, strategies for preventing this type of accident in an academic research laboratory using these hazardous gases are discussed.

Document Control Page	1. NREL Report No. NREL/TP-451-5756	2. NTIS Accession No. DE93018214	3. Recipient's Accession No.

4. Title and Subtitle

Stable, High-Efficiency Amorphous-Silicon Solar Cells with Low Hydrogen Content

5. Publication Date

August 1993

6.

7. Author(s)

S.S. Hegedus, J.E. Phillips

8. Performing Organization Rept. No.

9. Performing Organization Name and Address

Institute of Energy Conversion
University of Delaware
Newark, Delaware

10. Project/Task/Work Unit No.

PV241101

11. Contract (C) or Grant (G) No.

(C) XG-1-10063-4

(G)

12. Sponsoring Organization Name and Address

National Renewable Energy Laboratory
1617 Cole Blvd.
Golden, CO 80401-3393

13. Type of Report & Period Covered

Technical Report
1 March 1991 - 31 March 1993

14.

15. Supplementary Notes

NREL technical monitor: B. von Roedern

16. Abstract (Limit: 200 words)

This report describes a 21-month project to demonstrate amorphous-silicon (a-Si) solar cells with high stabilized conversion efficiency. The objective was to develop a research program spanning material issues (more stable a-Si and better a-SiGe alloys) and device issues (more stable a-Si-based solar cells) with the goal of high stabilized solar cell efficiency. The Institute of Energy Conversion (IEC) produced and analyzed the stability of a-Si films and solar cells with reduced hydrogen content (2%–6%). A thermodynamic model of defect formation was developed that describes the high-temperature degraded state of a solar cell. An analysis of bifacial current voltage and quantum efficiency results for a-SiGe p-i-n devices with transparent front and back contacts provided information about the influence of alloying and band-gap grading on hole and electron collection. IEC also studied the stability of graded and ungraded a-SiGe solar cells using bifacial devices to learn about the relative degradation of hole and electron collection, and concludes that degradation of the photoconductivity of a-SiGe materials does not agree with degradation observed in solar cells.

17. Document Analysis

a. Descriptors

high efficiency ; amorphous silicon ; hydrogen ; germanium ; photovoltaics ; solar cells

b. Identifiers/Open-Ended Terms

c. UC Categories

271

18. Availability Statement

National Technical Information Service
U.S. Department of Commerce
5285 Port Royal Road
Springfield, VA 22161

19. No. of Pages

70

20. Price

A04